Spring 2012

Alterations in brain connectivity after spinal cord injury using functional MRI

Yamin Ahmed Noor
New Jersey Institute of Technology

Copyright Warning & Restrictions

The copyright law of the United States (Title 17, United States Code) governs the making of photocopies or other reproductions of copyrighted material.

Under certain conditions specified in the law, libraries and archives are authorized to furnish a photocopy or other reproduction. One of these specified conditions is that the photocopy or reproduction is not to be "used for any purpose other than private study, scholarship, or research." If a, user makes a request for, or later uses, a photocopy or reproduction for purposes in excess of "fair use" that user may be liable for copyright infringement,

This institution reserves the right to refuse to accept a copying order if, in its judgment, fulfillment of the order would involve violation of copyright law.

Please Note: The author retains the copyright while the New Jersey Institute of Technology reserves the right to distribute this thesis or dissertation

Printing note: If you do not wish to print this page, then select "Pages from: first page # to: last page #" on the print dialog screen

ABSTRACT
ALTERATIONS IN BRAIN CONNECTIVITY AFTER SPINAL CORD INJURY USING FUNCTIONAL MRI

by

Yamin Ahmed Noor

Every year, approximately 50 people per million of inhabitants are inflicted by Spinal Cord Injury (SCI). The long-term impairment of the SCI patients has led researchers to investigate different rehabilitation and treatment efforts that require careful observations to be made on reliable markers. Presently, a number of neuropsychological assessments are used for SCI rehabilitation and research purposes. However, there is a need for the discovery of sensitive biomarkers that can be used to characterize SCI. Altered functional connectivity in the brain has been observed in a number of neurological patient populations. Hence, it was hypothesized that such alterations in brain connectivity occurs after SCI as well. In this study, functional magnetic resonance imaging (fMRI) was used to study brain functions while at rest on 23 healthy control subjects and 38 SCI subjects. Based on the level of injury, SCI subjects were divided into two groups of paraplegic and tetraplegic subjects, respectively. Independent component analysis (ICA) was performed on the three groups of subjects as well as the on the study population in order to approximate underlying brain networks. Corresponding spatial independent components obtained from the three groups demonstrated difference in spatial maps. Analysis of variance revealed group differences among the three groups in three neural networks – default mode network, right lateralized fronto-lateral network, and sensorimotor network. In addition, correlations were found between the neuropsychological assessment scores and connectivity strength of the locations that demonstrated difference. The results from this study which is preliminary in nature demonstrated alterations in brain connectivity in SCI patients. Furthermore, this study may provide information that can be used as biomarkers for SCI patient population.

ALTERATIONS IN BRAIN CONNECTIVITY AFTER SPINAL CORD INJURY USING FUNCTIONAL MRI

by
Yamin Ahmed Noor

A Dissertation
Submitted to the Faculty of
New Jersey Institute of Technology
in Partial Fulfillment of the Requirements for the Degree of
Masters in Biomedical Engineering

Department of Biomedical Engineering

May 2012

APPROVAL PAGE

ALTERATIONS IN BRAIN CONNECTIVITY AFTER SPINAL CORD INJURY USING FUNCTIONAL MRI

Yamin Ahmed Noor

Dr. Tara Alvarez, Thesis Advisor — Date
Associate Professor, Department of Biomedical Engineering, NJIT

Dr. Bharat Biswal, Committee Member — Date
Associate Professor, Department of Radiology, UMDNJ

Dr. Mesut Sahin, Committee Member — Date
Associate Professor, Department of Biomedical Engineering, NJIT

BIOGRAPHICAL SKETCH

Author: Yamin Ahmed Noor

Degree: Masters of Science

Date: May 2012

Undergraduate and Graduate Education:

- Masters of Science in Biomedical Engineering,
  New Jersey Institute of Technology, Newark, NJ, 2012

- Bachelor of Science in Biomedical Engineering,
  New Jersey Institute of Technology, Newark, NJ, 2011

Major: Biomedical Engineering

To my family and my friends.

ACKNOWLEDGMENT

I would first like to thank Dr. Bharat Biswal, for without you none of this would have been possible. I would like to thank Dr. Tara Alvarez for her shared passion and eagerness to learn more about the human brain with me. I would like to thank Dr. Mesut Sahin, who has unfailingly supported me since I was an undergraduate in the Biomedical Engineering Department. I would also like to thank Dr. Paul Taylor and Dr. Xin Di for their unremitting assistance. I want to especially thank Suril Gohel for helping me throughout the study with my most trivial problems.

TABLE OF CONTENTS

TABLE OF CONTENTS
(Continued)

Chapter **Page**

LIST OF TABLES

LIST OF FIGURES

LIST OF FIGURES
(Continued)

Figure **Page**

CHAPTER 1

INTRODUCTION

Spinal cord is part of the central nervous system which relays motor and sensory information between brain and peripheral nervous system (PNS). As a result, spinal cord injury (SCI) patients suffer from damage to neuronal pathways and demonstrate motor and sensory impairments. Globally, the number of SCI incidences range from 10.4 to 83 per million of inhabitants per year (Wyndaele and Wyndaele, 2006). Based on the neurological assessment after the injury, SCI can fully or partially disrupt the flow of information between the brain and the body. Almost half of the SCI patients suffer from tetraplegia (or quadriplegia), which is the paralysis of all four limbs and the body, and the rest are diagnosed with paraplegia, which affects the two lower limbs. SCI can also be classified as complete or incomplete based on behavioral scores which correspond to the amount of motor or sensory activity that occurs below the level of SCI.

Spinal cord is surrounded by the vertebral column. Nerves consisting of axons of afferent sensory neurons and efferent motor neurons enter and exit the spinal cord, respectively, through foramina in the vertebral column. The level of SCI is defined according to the foramina through which the peripheral nerves enter or exit the spinal cord. Therefore, if the SCI is in the fourth vertebrae of the thoracic region then the level of SCI is T4 which might be responsible for motor and sensory impairment in the torso.

Neurons in the afferent nerves receive sensory input from dermatomes whereas neurons in the efferent nerves innervate muscle units called myotomes. Usually, a one-to-one correspondence is present between the dermatomes and the afferent nerves. However,

the connectivity between efferent nerves and myotomes are more complex. Most afferent nerves innervate more than one muscle and most muscles are innervated by more than one afferent nerve. However, it is possible to determine the level of SCI by systematically examining the myotomes and dermatomes (Maynard et al. 1997). A number of measures of neurological damage can be generated from such systematical assessment which includes examining sensory and motor level for each side of the body. Such behavioral assessments are primarily used in studies involving treatment or rehabilitation after SCI.

The long-term impairment of the PNS in the SCI patients has led to different rehabilitation efforts. However, the ultimate goal lies within finding the clinically most effective treatment to remedy the effects of SCI. Although, presently, there is no remedy for SCI, recent discoveries suggest that the damaged neuronal pathways in SCI patients can be repaired (Schwab, 2002). The American Spinal Injury Association (ASIA) has developed elaborate guidelines for the neuropsychological assessment and characterization of SCI. The ASIA system assesses both, sensory and motor, performances and scores them. The system also has a provision for characterizing the SCI patients into five categories. While the ASIA scoring system is widely used, there is a need for carefully designed clinical trials in order to investigate the performance of such treatments which prerequisites the development of non-invasive biomarkers in order to quantify the effects of SCI on the functional connectivity of the cortical regions in the brain. In order to develop accurate and sensitive biomarkers involved with spinal injury it is imperative to understand the pathophysiological events following injury.

While the pathophysiology in SCI is not caused by lesions in the brain, a number of studies have reported cortical alterations in the brain after spinal injury (Frost et al.,

2003; Jones, 2000; Sanes et al., 2003, Sanes et al., 2007; Wu and Kaas, 1999). SCI damages the axons and, thereby, disrupts neuronal pathways between the brain and spinal cord. However, most of the neurons in the affected neural pathway survive the damage and remain receptive to synaptic input (Hains et al., 2003; Beaud et al., 2008; Tseng and Prince, 1996). Studies suggest that axonal regeneration is a potential mechanism for functional reintegration of the injured neurons into the neuronal pathway (Freund et al., 2006; Bareyre et al., 2004). Axonal regeneration increases access to neurotrophic support, which increases the potential of the survival of damaged cells and contributes to cortical reorganization. Alterations in functional connectivity have been observed in brain injuries such as stroke, traumatic brain injury, and multiple sclerosis (Giorgio et al., 2010; Rico et al., 2011). Such reorganization has been reported after SCI as well (see review by Kokotilo et al., 2009).

Functional MRI (fMRI) has also been used to study cortical reorganization after SCI. fMRI measures the blood-oxygen-level-dependent (BOLD) signal which can be correlated to the neural activity. A number of task-based studies have used fMRI to determine cortical reorganization in SCI patients. Since SCI patients are unable to perform most motor tasks, attempted or imaginary motor tasks are employed in most task-based SCI studies. Cramer et al. (2005) studied brain activation using fMRI for an attempt leg movement and an imaginary leg movement where they found reduced volume of activation as well as abnormal activation in SCI patients. Other studies using different tasks conformed to such conclusion regarding the abnormal activation pattern in SCI patients (see review by Kokotilo et al., 2009).

Resting-state fMRI is being widely used to study the brain connectivity without

any priori hypothesis. To our knowledge, resting-state fMRI data has not been analyzed to identify biomarkers involved with SCI. At resting-state, large-amplitude spontaneous low-frequency (<0.1 Hz) fluctuations in the fMRI signal can be found which can be temporally correlated across functional brain regions (Biswal et al., 1995). A number of methods are in use to determine brain-connectivity from resting-state fMRI data.

A number of methods are being used to evaluate resting state connectivity which includes spatial Independent Component Analysis (ICA), seed based correlation, and small-world analysis. Resting state networks are often revealed by ICA. ICA is applied to fMRI data in order to determine spatially independent brain networks. This method is useful to study brain activity at resting state in both healthy controls and different types of patient groups (Calhoun et al., 2009). Differences in functional connectivity can be determined by comparing the ICA of the healthy controls with that of the patients.

In this study, resting-state fMRI data is analyzed in order to determine the extent of alterations in functional connectivity after SCI. ICA is performed on resting-state fMRI data of a healthy control group as well as two groups of SCI patients – tetraplegia and paraplegia. Differences in connectivity strength among the three groups are determined from the spatial ICA maps. It is found that, three spatial IC networks demonstrate significant differences among the three groups which can provide useful clinical or cognitive information about SCI patient population. Furthermore, such distinct characteristics can be useful biomarkers for SCI patient population.

CHAPTER 2

BACKGROUND OF SPINAL CORD INJURY

The nervous system can be divided into the Central Nervous System (CNS) and Peripheral Nervous System (PNS). The CNS consists of the brain and the spinal cord whereas PNS encompasses the motor and sensory neurons throughout the body. Spinal cord relays motor and sensory information between brain and PNS. As a result, an injury to the spinal cord disrupts the flow of information from and to the brain and the PNS. There are various ways of characterizing SCI. For example, SCI may be characterized depending on the anatomical location of the injury on the vertebral column or the neurological level of spinal roots within the vertebral column. Furthermore, the sensory and motor assessments of the SCI patient may be used to characterize the pathology. The neuropsychological assessments might also be used to characterize SCI to be complete or incomplete. The American Spinal Injury Association (ASIA) has developed elaborate guidelines for the neuropsychological assessment and characterization of SCI.

2.1 Anatomical and Neurological Levels of SCI

The spinal cord is surrounded by the vertebral column. The vertebral column consists of bony segments called vertebra. Anatomically, the vertebral column can be divided into four regions as represented in Figure 2.1. The four regions are cervical, thoracic, lumbar, and sacral regions. There are seven cervical, twelve thoracic, five lumber, and five sacral vertebrae. The neurological level of spinal cord is not necessarily the same as the vertebral column. Different neurological levels can be defined by spinal roots that enter

or exit the vertebral column through space between two vertebras called foramen. For example, the neurological C8 cord is located at the anatomical C7 vertebra. Similarly, the neurological T12 cord is located at the anatomical T8 vertebra. Moreover, the lumbar cord is located between anatomical T9 and T11 vertebrae whereas the sacral cord between the T12 to L2 vertebrae. Therefore, the anatomical vertebral level and neurological spinal cord level are not necessarily the same.

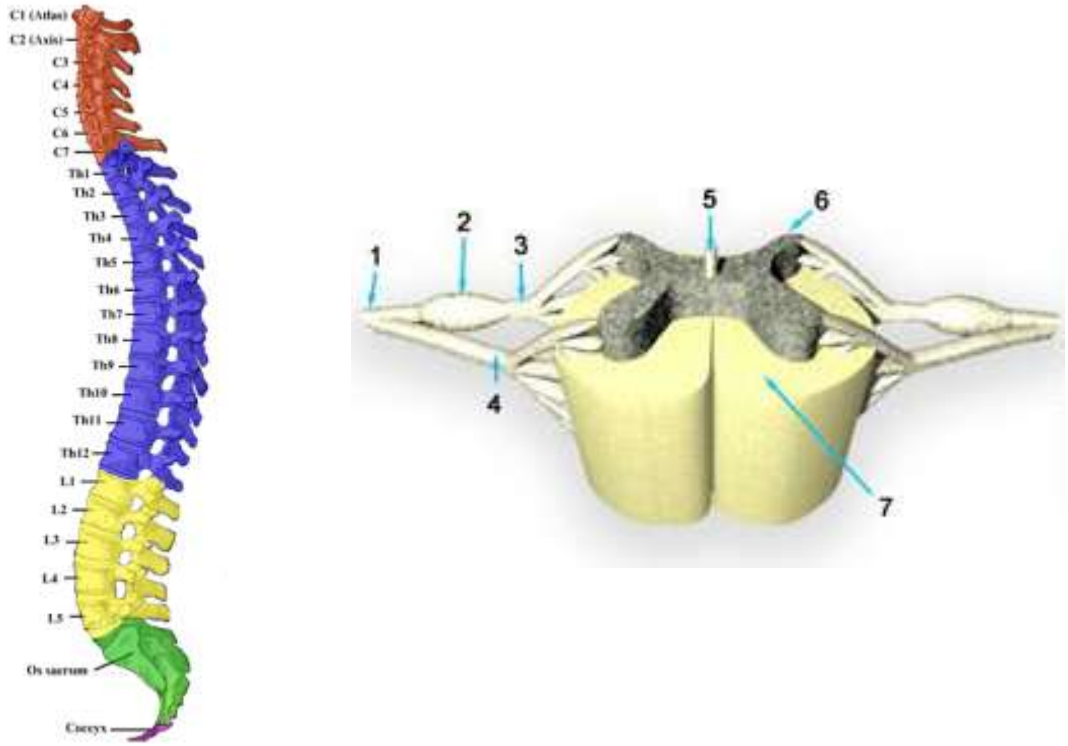

Figure 2.1: Vertebral column (left) and spinal cord within vertebral column (right). The denoted parts in the spinal cord image are – 1. Spinal Nerve, 2. Dorsal Root, 3. Dorsal Root (Sensory), 4. Ventral Root (Motor) Ganglion, 5. Central Canal, 6. Grey Matter, 7.White Matter. (http://en.wikipedia.org/wiki/File:Gray_111_-_Vertebral_column-coloured.png), (http://www.apparelyzed.com/spinalcord.html).

2.2 Sensory and Motor Levels of SCI

Neurons in the afferent nerves receive sensory input from dermatomes, which are patches of skin that innervate the nervous system, whereas neurons in the efferent nerves

innervate muscle units called myotomes, which are muscle groups that are innervated by the nervous system. Usually, a one-to-one correspondence is present between the dermatomes and the afferent nerves. However, the connectivity between efferent nerves and myotomes are more complex. Most afferent nerves innervate more than one muscle and most muscles are innervated by more than one afferent nerve. However, it is possible to determine the level of SCI by systematically examining the myotomes and dermatomes (Maynard et al. 1997).

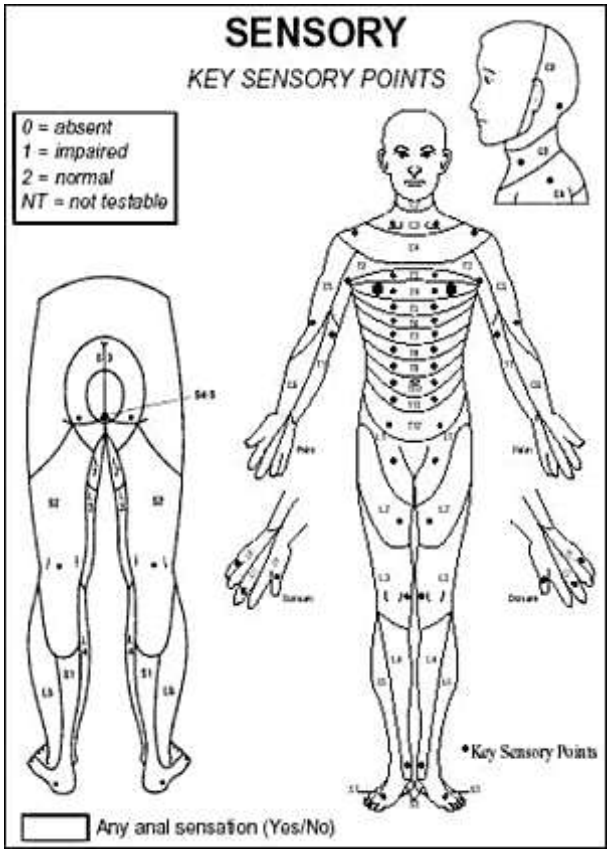

Figure 2.2: Dermatomes as assigned by ASIA (Maynard et al. 1997).

Figure 2.2 represents the ASIA location of the dermatomes across human body. Depending on the plasticity of the nervous system, the dermatomes may expand or contract. Dermatomes are named after the neurological level of spinal cord that are

innervated by the dermatome. For example, the C2 dermatome is located across the occiput and the top part of the neck whereas lower part of the neck to the clavicle is c C3, and the skin patch below clavicle is C4. The motor levels of SCI are determined from the assessment of ten muscle groups. The muscle groups consist of the biceps, triceps, flexors, and abductors in the arm and the hand, the flexors and the extensors in the leg and the foot, and the anal sphincter which is innervated by neurological levels of SCI located in the sacral region. The anal sphincter is located at the very end of the spinal cord, if a SCI patient can voluntarily contract the muscle; the pathology is defined as motor incomplete injury. It must be noted that the motor level of SCI defined by ASIA has been criticized to be an oversimplification of the actual pathology because muscles are usually innervated by more than one spinal cord level.

2.3 Complete and Incomplete Injury

Based on the voluntary motor or conscious sensory responses, SCI is commonly described as “complete” or “incomplete”. A SCI is defined to be complete if the voluntary movement and sensory excitation is utterly absent below the neurological level of SCI. However, the characterization of SCI as “complete” or “incomplete” can be ambiguous if partial preservation of sensory or motor function occurs. Also, there are cases of lateral preservation where the motor and sensory functions in one side of the body remains intact although becomes impaired on the other side. Also, rehabilitation efforts have led to partial recovery from SCI. Therefore, defining a SCI to be “complete” or “incomplete” can be deemed to be arbitrary in certain cases. Though ASIA has implemented a criterion which states that, if a SCI patient does not have any neurological

function below the neurological level of injury then the person may deem to have “complete” SCI.

Since the axons and some neural pathways stay intact in spite of the absence of motor and sensory functions below the injury site, some clinicians define "complete" SCI when there is the lack of axons crossing the injury site. However, clinical and animal studies suggest that a vertebrate with no function below the injury site may recover certain neurological functions after the spinal cord has been decompressed, or treated. Therefore, the classification of SCI as “complete” and “incomplete” is not widely accepted.

2.4 Characterization of SCI

As it can be inferred from the aforementioned discussion, the terminology associated with SCI levels, severity, and classification can be confusing. Therefore, researchers have been trying to identify biomarkers associated with the characterization of SCI. Some studies have characterized SCI by the thickness of the spinal cord (Freund et al, 2011). Other studies have attempted to examine the brain for useful biomarkers (Frost et al., 2003; Jones, 2000; Sanes et al., 2003, Sanes et al., 2007; Wu and Kaas, 1999). Henderson and colleagues (Henderson et. al, 2011) tested two hypotheses regarding the mechanism of cortical reorganization. The first hypothesis was that there are latent synaptic connections between the brain regions which are merely unmasked following SCI. The other hypothesis suggests that the absence of signal triggers cortical reorganization by inducing the formation of novel synaptic connections. Henderson and colleagues (Henderson et. al, 2011) combined anatomical information with the functional

results of displacement to suggest that the cortical reorganization is a combination of both of the mechanism where smaller displacements might be due to the unmasking of latent synaptic connections and larger displacements might be due to the formation of novel connections.

The activation in the primary motor cortex during an imagining task of the lower limb movement as studied by Gustin and colleagues (Gustin et. al, 2010), demonstrate the ability of the primary motor cortex to be activated in spite of the impairment of the lower limbs in the SCI subjects. Studies have reported conflicting results regarding the activation of the primary motor cortex in the past as discussed by Kokotilo and colleagues (Alkadhi et al, 2005; Bruehlmeier et al, 1998); Curt et al., 2002a, 2002b; Mattia et al., 2006). The particular imagining task in Gustin and colleague's (Gustin et. al, 2010) study corresponds to the efferent pathway from the brain. The lower limb sensation tasks performed by Henderson and colleagues (Henderson et. al, 2011) and Freund and colleagues (Freund et. al, 2011) did not yield any significant activation in the cortical region of the brain which can be attributed to the absence of the afferent pathway to the brain. Henderson and colleagues (Henderson et. al, 2011) found that the functional region corresponding to finger sensation are displaced towards the midline which is near the cortical region that correspond to the lower limbs. Moreover, behavioral study on the SCI subjects in the study by Henderson and colleagues (Henderson et. al, 2011) reported that the SCI subjects perform finer upper limb activity after their injury compared to before injury. Such behavioral characteristics may be attributed to altered functional connectivity in the primary somatosensory cortex as reported by Henderson and colleagues (Henderson et. al, 2011). In addition, Freund and colleagues (Freund et. al,

2011) reported that both, the motor task of hand-griping and the sensory task of median nerve stimulation, showed higher activity in regions corresponding to the leg with in the primary motor cortex. Therefore, the results from the three studies may suggest that, although the efferent activity corresponding to lower limbs in SCI subjects are strengthened, the afferent impairment of the lower limbs results in cortical reorganization in the primary motor cortex resulting in recruitment of regions corresponding to the lower limbs by functional regions corresponding to the upper limbs.

The contrasting shift in activation in the direction of the deafferented lower limb representation may be explained by the timeline of SCI. Lotez and colleagues (Lotze et al, 2006) reported that activation displacement toward the deafferented lower limb in the SCI subjects correlates with the time since the injury which supports the deduction made from the three reviewed studies. However, Bruehlmeier and colleagues (Bruehlmeier et. al, 1998) reported that the shift in brain activation may be influenced by level of SCI. Kokotilo and colleagues (Kokotilo et. al, 2009) supports the aforementioned report based on their literature review which indicated that the type of activation shift occurring after SCI may depend on level of injury. Completeness and level of injury in SCI affect the amount, quality, or influence of afferent input to the brain which is important in motor control. Individuals with deafferentation lower limbs are often not capable of performing complex movements which require coordination between several joints accurately (Jeannerod et al., 1984) as well as controlling force output accordingly (Jeannerod et al., 1984; Nowak et al., 2003). Therefore, the importance of sensory afferent feedback to movement is very much. The lack of such afferent sensory information in SCI subjects can lead to the cortical reorganization and therefore, irregular brain activation after SCI.

The above mentioned neuroimaging studies are task-based which means that participants were given sensory input or asked to move or attempt to move. Since a bulk of the SCI patients is unable to receive sensory input or perform voluntary motion, resting-state fMRI may be advantageous in studying SCI pathology.

CHAPTER 3

FOUNDATIONS OF FUNCTIONAL MAGNETIC RESONANCE IMAGING

Magnetic Resonance Imaging (MRI) has become one of the most used imaging modalities for research and clinical purposes because of its non-invasive nature, high spatial resolution resulting in excellent tissue contrast, and absence of ionizing or radioactive agents. MRI is based on a principle called Nuclear Magnetic Resonance (NMR). Flex Bloch and Edward Purcell discovered NMR in 1946 which helped researchers to explain different chemical properties of materials. Hermann Carr applied the principles of NMR to obtain one-dimensional MRI in 1952. In the 1970s, Paul Lauterbur and Peter Mansfield were able to obtain two and three-dimensional MR images using the principles of NMR which remains the precursor of present day MRI techniques. Both, Lauterbur and Mansfield, were awarded with the Nobel Prize in 2003 in Medicine for their work towards developing MRI. Functional MRI (fMRI) is a special type of MRI technique where reasonably fast rate of imaging and a specific contrast allow for the estimation of temporal activity across the brain. In the recent times, fMRI has become a popular technique in different fields of neuroscience research. This chapter includes description of how the MR signals are generated and localized during MRI and how the principle can be applied to acquire fMRI.

3.1 Generation of MR Signal

Human body is composed of approximately 70% water. Each water molecule contains two hydrogen atoms. As a result, hydrogen is the most abundant element in human body.

Hydrogen atom is a structurally simple element because it is constituted of a proton and an electron only. Although water is not an ionic molecule, the electronegativity of oxygen and small size of hydrogen makes it polar in nature. Polar molecules are affected by magnetic fields. Therefore, abundance of water in human body and polarity of water makes it a useful and suitable imaging molecule. Abundance of water within different types of tissues and body fluids varies distinctively. There is a direct relationship between the amount of MR signal generated and water concentration of the tissue or fluid type of interest. Hence, in MR images we are able to contrast between different tissue types as well as identify tissue types based on intensity.

NMR can be explained by the quantum properties of nuclei. Nuclei are composed of protons and neutrons. Where neutrons are electromagnetically neutral, protons are considered to have electrical charge. The number of protons in the nucleus defines atomic number of an element. Nuclei with odd atomic number possess angular momentum which is also known as spin. A nucleus with spin rotates about its axis, similar to the rotations of planets in the solar system, which results in magnetic moment due to the presence of electrical charge. Because of such magnetic moment, in the presence of strong magnetic field such nucleus with magnetic moment aligns itself to the field as shown in Figure 3.1. There is a direct relationship between the nucleus and the strength of its magnetic moment.

Hydrogen nucleus is the simplest of all elements since it merely has a proton in its nucleus. However, hydrogen nucleus has the strongest magnetic moment and is widely used to explain NMR. The magnetic moment of a proton, or in case of hydrogen its

nucleus, is proportional to its spin angular moment which can be represented by equation 3.1,

$$\boldsymbol{\mu} = \gamma \boldsymbol{J} \qquad [3.1]$$

where $\boldsymbol{\mu}$ is the magnetic moment, $\boldsymbol{J}$ is the spin angular moment, and γ is a constant known as gyromagnetic ratio which is a property of the nucleus. The energy level and orientation of the spinning protons can be characterized by a specific quantum number. In a collection of protons, as in Figure 3.1, when an external magnetic field, $\boldsymbol{B_o}$, is absent, the orientations of magnetic moment of the protons vary randomly. When the protons are placed in a uniform magnetic field, they align themselves with or against the external magnetic field, $\boldsymbol{B_o}$. This phenomenon is known as paramagnetic polarization. In room temperature, protons that align themselves in the direction of $\boldsymbol{B_o}$, slightly outnumbers the protons that align themselves in the direction opposite of $\boldsymbol{B_o}$. As a result, an overall net magnetization vector, $\boldsymbol{M_o}$, evolves which is parallel to $\boldsymbol{B_o}$ and is the basis for MR signal.

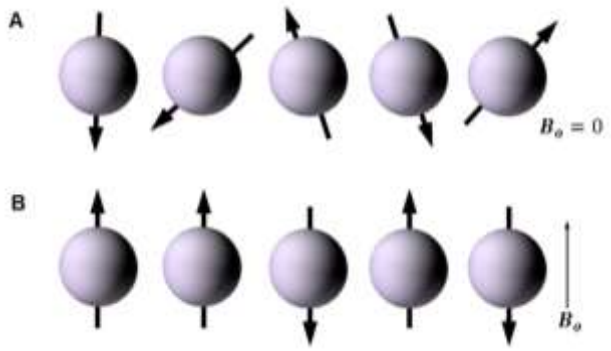

Figure 3.1: Spin characteristics of proton with and without applied magnetic field. (a) Randomly aligned individual spins in absence of magnetic field. (b) Spins aligned in either the same or in the opposite direction of the applied magnetism. Hence, a net magnetic moment is in the direction of applied magnetic field.

While the protons align themselves along the direction of $\boldsymbol{B_o}$, they rotate about their own axes as well as precess about axes parallel to the direction of $B_o$as shown in

Figure 3.2a. The frequency of precession is called Larmor Frequency. Larmor Equation (equation 3.2) expresses the relationship between the magnetic field, $\boldsymbol{B_o}$, and the Larmor frequency, ω_o.

$$\omega_o = \gamma B_o \quad [3.2]$$

The gyromagnetic ratio of hydrogen nucleus is 42.57 MHz/T. Therefore a magnetic field of strength 1.0 Tesla, the Larmor Frequency ω_o= 42.57 MHz. For a constant magnetic field and known gyromagnetic ratio, elements can be selectively excited in order to generate varying MR signals. In case of MRI such excitation is performed by the application of a radio frequency (RF) pulse which has the same frequency as the precession frequency of the proton. This phenomenon is known as resonance and, hence, the signal is known is magnetic resonance (MR) signal. Resonance is the tendency of a system to maximally oscillate in the presence of a specific frequency called resonance frequency of that system. In MRI, resonance is a critical step where the energy of RF wave is transferred to protons in precession; consequently, Larmor frequency is the resonance frequency.

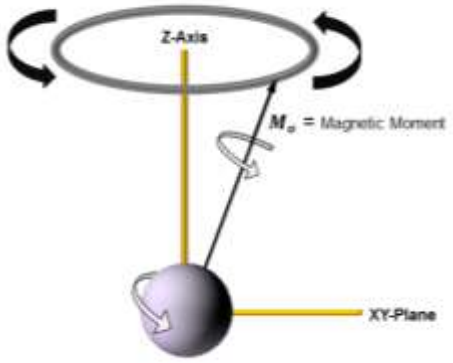

Figure 3.2: Proton in precession in the presence of RF pulse and external magnetic field. Due to the added energy, the net magnetic moment shifts to the transverse plane from the longitudinal plane.

By convention, the magnetic field, $\boldsymbol{B_o}$, is parallel to the Z-axis in the three-dimensional space. The net magnetization vector, $\boldsymbol{M_o}$, can be decomposed into two components, $\boldsymbol{M_{XY}}$ and $\boldsymbol{M_Z}$ along the X,Y-plane and the Z-axis respectively. In the presence of $\boldsymbol{B_o}$, after equilibrium has been reached, $\boldsymbol{M_o}$ is equal to $\boldsymbol{M_Z}$ or the longitudinal magnetization vector as a result of paramagnetic polarization; consequently, $\boldsymbol{M_{XY}}$ or the transverse magnetization vector zeros at equilibrium. When RF pulse is applied to this system, it acts as a second external magnetic field, $\boldsymbol{B_1}$, which is perpendicular to that of $\boldsymbol{B_o}$ as shown in Figure 3.2b. Depending on the strength and duration of $\boldsymbol{B_1}$, the magnitude of $\boldsymbol{M_Z}$ decreases while the magnitude of $\boldsymbol{M_{XY}}$ increases as $\boldsymbol{M_o}$ transitions between parallel and anti-parallel states. The angle at which $\boldsymbol{M_o}$ rotates away from $\boldsymbol{M_Z}$ is called the flip angle, θ, which is proportional to the strength and duration of $\boldsymbol{B_1}$. The flip angle depends on the duration and strength of the RF pulse according to equation 3.3,

$$\theta = \gamma B_1 t \qquad [3.3]$$

where t is the duration of the RF pulse. If $\boldsymbol{B_1}$ is applied indefinitely, then $\boldsymbol{M_o}$ rotates away from the Z-axis and through the XY plane towards the anti-parallel direction or negative Z-axis. Displacement of $\boldsymbol{M_o}$ to the XY-plane results in changes within the magnetic flux which allows for overall variation in magnetization to be measured. Optimal results are expected for largest transverse magnetization as a result of application of 90° RF pulse. After the conclusion of RF pulse, the second external magnetic field $\boldsymbol{B_1}$is withdrawn and the magnetization vector $\boldsymbol{M_o}$ gradually return back to the equilibrium while emitting MR signals. The MR signals and the rate of relaxation are proportional to the number of excited protons in the sample tissue type.

3.2 Types of MR Signal

The aforementioned generation of MR signals merely represents the local density of protons; also known as proton-density image. Hence, signal intensity increases with the presence of protons at a higher concentration. While proton-density images can be useful, MRI can be manipulated to weigh a number of biological properties of tissue. After the withdrawal of $\boldsymbol{B_1}$, $\boldsymbol{M_o}$ returns to its equilibrium state along the z-axis which is known as the relaxation process. The relaxation process can be characterized from two perspectives –regeneration of net magnetization along the Z-axis; and net magnetization decay along the XY-plane.

The regeneration of the longitudinal magnetization is longer of the two relaxation times because each of the nuclei excited by the RF pulse needs to release energy to the local tissue or the lattice which further depends on the structure of the tissue or the lattice. $T_1$is defined as the relaxation time for longitudinal magnetization vector $\boldsymbol{M_Z}$. By convention, $T_1$is the time taken by $\boldsymbol{M_Z}$ to recover to 63% of its original value following the application of the RF pulse (Figure 3.3(left)). Equation 3.4 represents the relationship between T_1 and M_Z,

$$M_Z(t) = M_o(1 - e^{-t/T_1}) \qquad [3.4]$$

where t is the instantaneous time and $M_Z(t)$is the magnitude of longitudinal magnetization vector at time t. The strength of the magnetic field, $\boldsymbol{B_o}$, increases with increase in Larmor frequency which also increases T_1. As stated earlier, T_1 depends on the tissue type and, thereby, varies for different tissue structures. In addition to the precession and rotation of nuclei, molecules, as a whole, exhibit motion and vibration. Larger molecules move slowly which exhibit low vibrational frequencies which are

clustered within lower range of the frequency spectrum. Smaller molecules exhibit vibrational frequencies throughout the frequency spectrum. Energy transfer is the most efficient when the precession frequency of the excited spins overlaps with the vibrational frequency of the tissue.

The decay of transverse magnetization occurs at a rate, much higher, than the longitudinal magnetization recovers. This decay is a result of the loss of phase coherence of the spins caused by inhomogeneity in the local magnetic field, which is a property of the tissue. This phenomenon is also known as spin-spin interaction. The decay is characterized by the time, T_2, taken by the transverse magnetization vector to decay to 37% of its peak value (Figure 3.3(right)). The relationship between $T_2$and M_{XY} can be represented by equation 3.5,

$$M_{XY}(t) = M_o e^{-t/T_2} \quad [3.5]$$

where t is the instantaneous time and $M_{XY}(t)$is the magnitude of transverse magnetization vector at time t.

Regardless of the software and the hardware efforts, in practical conditions it is literally impossible to achieve perfectly homogeneous $\boldsymbol{B_o}$. Similar to the T_2 relaxation, the net average magnetization decreases exponentially (Figure 3.3(right)) following the withdrawal of the RF pulse as a result of the loss of phase coherence of the spins caused by inhomogeneity in the local magnetic field as well as $\boldsymbol{B_o}$. Hence, this phenomenon exhibits the total decay of the transverse magnetization vector, which includes the consequences of magnetic field inhomogeneity as well as of spin-spin interactions, and is defined by relaxation time T_2^*, where $T_2^*<T_2$.

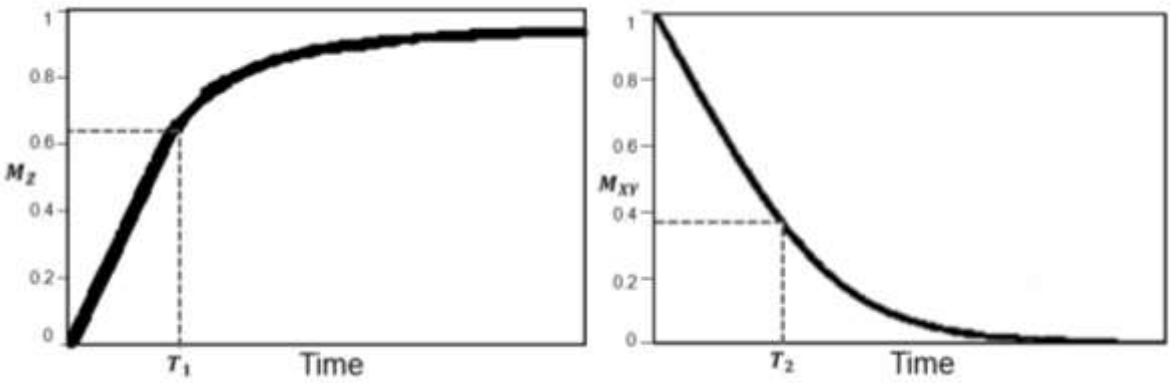

Figure 3.3: T_1(left) and T_2(right) relaxation.

The motion and size of the molecules as well as the interaction between molecules defines the duration of the relaxation times. For example with soft tissue T_2 can be almost 10 times faster than T_1. Biologically, T_1 ranges from 0.1 to 1 second for soft tissue and from1 to 4 seconds in aqueous tissue such as cerebrospinal fluid (CSF). Again, aqueous liquids such as CSF exhibit longer T_2 as a result of rapid molecular motion which cancels the local magnetic inhomogeneity. With increase in the size of molecule, T_2 decay also increases and ranges from 10 to 100 milliseconds. Such differences in the relaxation times can be utilized to obtain high definition and high contrast in MR images. Although $\boldsymbol{B_o}$ directly impacts T_1-relaxation time, it has no effect on T_2-decay. In summary, the relaxation times are functions of the tissue characteristics and $T_1 > T_2 > T_2^*$. Since spin density is a fundamental property of tissue, it can be exploited to obtain different MR signals which can be used to contrast between different types of tissues.

3.3 Localization of MR Signal

The discussion of MRI so far included the physics of MR signal which was introduced by Bloch and Purcell in 1946. The utility of MRI, however, lies in the ability to localize the

MR signal to anatomical locations, which was developed by Mansfield and Lauterbur. This is performed by emphasizing the differences among spin densities, and T_1 and T_2 relaxation times, altering the order, polarity, timing, and repetition frequency of the RF pulses, and applying magnetic field gradients. Appropriate combinations of one or more RF pulses and gradients with intervening periods of recovery are called pulse sequences. Each pulse sequence consists of repetition time (TR), echo time (TE), flip angle, the number of excitations, bandwidth, and acquisition matrix. Spin-echo is one of the widely used pulse sequences applied in modern MRI techniques.

Two coils of wire, wound in opposite direction, can be placed around the $\mathbf{B_0}$ field to superimpose a magnetic field gradient which would result in higher field strength for one end of the magnet than the other. Therefore, identical nuclei will precess at different Larmor frequency as a predicted by Larmor equation. The deviation in frequency is

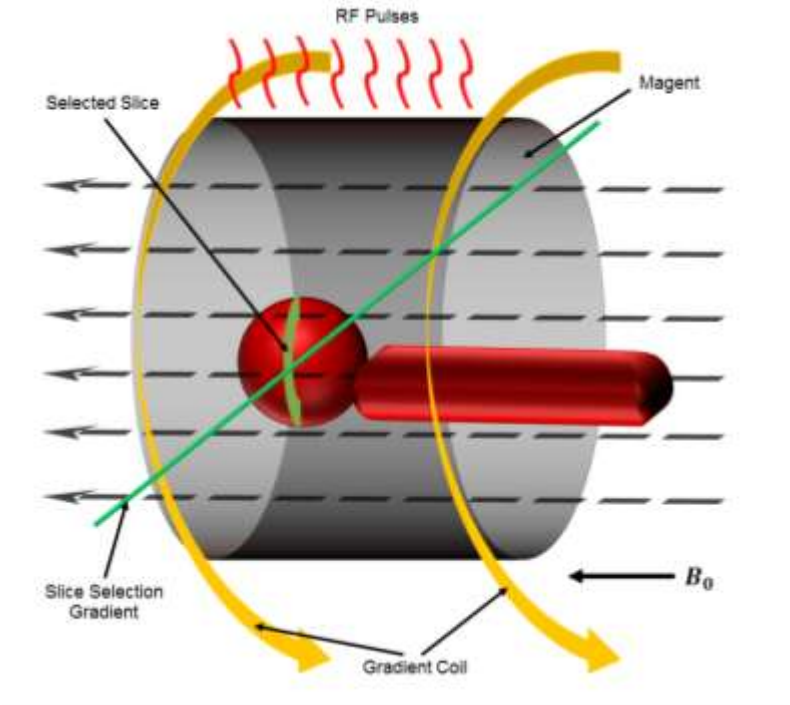

Figure 3.4: Selection of a slice along the Z-axis by the application of RF pulse with specific frequency and hence resonating protons situated within a desired slice.

proportional to the distance of the center of the gradient coil to the nuclei as well as the current flowing through the coil. As a result, if the gradient is switched on, then a sole RF pulse applied to the field will allow a thin plane perpendicular to the longitudinal axis at the center of the patient's brain to absorb the energy. Throughout the rest of the brain volume the absence of Larmor frequency will result in the lack of excitation for resonance to occur. Thereby, a slice with the thickness determined by the magnetic field gradient strength can be selected from the brain volume. This is how researchers activate the one slice within the brain volume at a time and avoid receiving overlapping data. The phenomenon is represented in Figure 3.4.

Three magnetic field gradients are placed, orthogonal to each other, inside the bore of the magnet which generates the external magnetic field $\mathbf{B_o}$ as illustrated in Figure 3.6. The gradients are used to encode spatial information along the three planes - axial (XY), sagittal (YZ), and coronal (XZ). After selecting a slice with the application of RF pulse, another gradient is switched on to spatially encode the excited protons in the slice along one of X- or Y-axis. Similar to the concept of selecting Z-slice, the gradient of the magnetic field forces all of the nuclei along the axis to precess at slightly different Larmor frequencies. Ideally the intensity of signal at each frequency is proportional to the number of protons in the corresponding column. This step is also known as phase-encoding step.

Following the phase encoding gradient, the frequency encoding gradient is turned on right before the receiver is turned on and it stays on while the fMRI signal is acquired by the receiver. The captured signal is formed as a result of the interference pattern of the different frequencies. After selecting a slice and frequency encoding the voxels within the

slice, the phase of the spins at one end of the gradient is different than those at the other end because of the difference in precessing frequency as a result of magnetic gradients. After switching of the frequency encoding gradient, spins precess at the same angular frequency, however, are not in phase with other anymore. Such a phenomenon is called phase memory. The phase encoding gradient, applied orthogonally to the other two gradients, does not change the frequency of the received signal because it is turned off during the acquisition of the signal. However, the phase memory maintains relative phases throughout the slice. Hence, the three dimensional location of the signal is modulated through the pulse sequence.

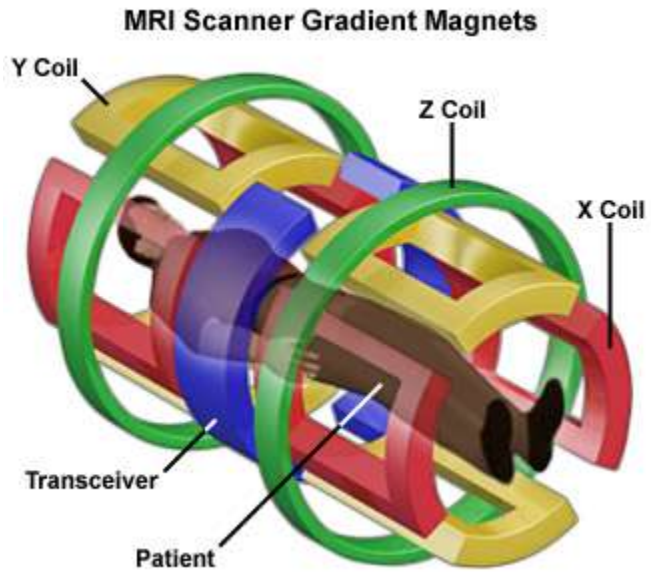

Figure 3.5: X, Y, and Z coils, placed orthogonal to each other. The RF coil is placed above the anatomical region to be imaged, i.e. bird-cage RF coil will be placed on top of the head in order to capture brain MRI. (http://www.medwow.com/articles/wp-content/uploads/2011/05/mri_magnets.jpg)

3.4 Echo Planar Imaging

Echo Planar Imaging (EPI) is fast imaging technique. EPI is a single-shot technique where the whole brain image is captured within a TR. A single-shot EPI begins with a 90° flip as a result of the RF pule which is followed by the acquisition of the data which is followed by a 180° echo-producing RF pulse. Multiple echoes provided by EPI pulse sequence allows for the capture of NMR signals through a single shot. However, the image clarity and resolution are compromised in order to produce the echo-planer images. Usually, EPI matrices are 64 x 64 or 128 x 64 as opposed to 256 x 256 or 512 x 512. Regardless, the ability of EPI to take almost real-time images have proven to be very useful for it can acquire images as fast as 64 per second in a single slice or an entire brain at a rate of 2 per second.

3.5 Instrumentation

The physics of NMR is the basis for MRI. Most of the components used in a MRI machine have already been discussed. A modern MRI machine is consisted of a super conductive magnet, a RF coil, and a gradient coil. The super conductive magnet is about 1 meter in diameter and 2-3 meters in length and it is an electromagnet. In order to increase the electromagnetism of the magnet, it is surrounded by liquid helium which is surrounded by liquid nitrogen containers with vacuum insulation barriers.

The superconductive magnet is designed to achieve extremely high magnetic field strength. While clinical MRI systems have magnets with field ranging from 0.3- to 3.0-Tesla, clinical research magnets range from 3.0- to 7.0-Tesla. The extremely high magnetic field is generated at a high cost of power. Inside the magnet is present a

shimming coil which increases the homogeneity of the magnetic field and, thereby, reduces artifacts. Again, the gradient coils are placed inside the magnet bore which are able to produce linear gradient magnetic fields. The RF coils creates the second magnetic field, $\mathbf{B_1}$. In most cases a bird-cage coil is used (Figure 3.5) for RF pulse which is placed closer to the brain. Furthermore, there are control interfaces, RF source, detector and amplifier, A/D converter, pulse programmer, computer system, gradient power supplies, and image display for the MR system.

3.6 Functional Magnetic Resonance Imaging

Functional magnetic resonance imaging or functional MRI (fMRI) is an MRI technique that measures brain activity. At its core, fMRI uses the blood-oxygen-level-dependent (BOLD) signal, which was discovered by Seiji Ogawa in 1991. fMRI can be used to map neural activity in the brain or spinal cord by imaging the change in blood flow which is related the activity in the brain. fMRI is based on the same principles as MRI, however, it contrasts the change in magnetization between oxygen-rich and oxygen-poor blood. Usually EPI is implemented in fMRI in order to have a reasonable temporal resolution. Although, fMRI can localize activity to within millimeters its spatial resolution is compromised.

CHAPTER 4

INDEPENDENT COMPONENT ANALYSIS

TO STUDY FUNCTIONAL BRAIN CONNECTIVITY

Among different computational methods, Independent Component Analysis (ICA) is one of the most widely used techniques for resting-state fMRI studies. ICA is a blind source separation method. ICA is used for separating statistically independent non-Gaussian source signal from a multivariate signal. ICA is widely used in analyzing resting-state fMRI data. There is no priori hypothesis in resting-state. Hence, ICA is a useful tool for separating the fMRI data to uncover underlying neural networks in the brain. On a single fMRI scan, two types of ICA may be performed – temporal and spatial. Temporal components are obtained from temporal ICA whereas spatial components are obtained from spatial ICA. In the context of resting-state fMRI, spatial ICA is especially useful because it can uncover statistically independent neural networks which may consist of anatomically distant yet functionally connected regions in the brain. Spatial ICA can be performed on a group of resting-state fMRI scans to obtain highly significant independent components. The larger the population size, the higher the significance of group independent components is. Group independent components can be back-projected onto individual scan to obtain spatially independent component specific to the scan for that independent component of interest. Hence, statistical analysis may be performed on groups of different populations to study group differences.

4.1 Principles of ICA

ICA is a data-driven method. The usefulness of ICA lies in its ability to uncover source signals from a multivariate signal under simple assumption. ICA is often explained in terms of the "cocktail party" example. If two people are speaking simultaneously in the same room and there are two microphones located at two different locations receiving the mixture of their speech then there will be two recorded signals which are denoted as $x_1(t)$ and $x_2(t)$ where t is the time index. It can be assumed that each of $x_1(t)$ and $x_2(t)$ is the weighted sum of the source speech signals $s_1(t)$ and $s_2(t)$, respectively, which can be represented by Equations 4.1 and 4.2, respectively.

$$x_1(t) = a_{11}s_1(t) + a_{12}s_2(t) \quad [4.1]$$

$$x_2(t) = a_{21}s_1(t) + a_{22}s_2(t) \quad [4.2]$$

where a_{11}, a_{12}, a_{21}, and a_{22} are parameters which are dependent on distances of the receivers from the sources. Equations 4.1 and 4.2 can be combined and expressed in matrix form where $\boldsymbol{x}$ and $\boldsymbol{s}$ are vectors of received signal and source signal respectively and $\boldsymbol{A}$ is a mixture matrix containing all the parameters (Equation 4.3).

$$\boldsymbol{x} = \boldsymbol{A}\boldsymbol{s} \quad [4.3]$$

Traditionally, it is not possible to solve Equation 4.3 for $\boldsymbol{s}$ without the knowledge of $\boldsymbol{A}$. However, it is possible to use ICA to make assumptions about the mixture matrix $\boldsymbol{A}$, and, thereby, estimate $\boldsymbol{s}$ by knowing $\boldsymbol{x}$. In order to do so, $\boldsymbol{x}$ and $\boldsymbol{s}$ need to be considered random variables. The primary assumption for ICA is that the components $s_i$are

statistically independent. The other assumption for ICA is that the independent components (IC) have non-Gaussian distribution.

4.2 Application of ICA in fMRI Analysis

As mentioned earlier, spatial ICA is applied on resting-state fMRI to uncover independent neural networks. In spatial ICA, fMRI data sets are modeled to be a linear mixture of spatially independent components which include both, Gaussian noises and brain activation signals. Therefore, the signal model of the spatial ICA can be presented as shown in Equation 4.4 –

$$\boldsymbol{x}(l,t) = \boldsymbol{A}\boldsymbol{s}(l,t) \quad [4.4]$$

where $0 < l < L$ is the index of voxel and $0 < t < N$ is the index of time-point. Therefore, $\boldsymbol{s}(l,t) = \{s_1(l), s_2(l), \dots, s_N(l)\}$ is a set of spatially independent components and $\boldsymbol{x}(l,t) = \{x_1(l), x_2(l), \dots, x_N(l)\}$ is a set of observed brain images at different time-points. Equation 4.5 can be rewritten to be

$$\boldsymbol{s}(l,t) = \boldsymbol{A}^{-1}x(l,t) = \boldsymbol{W}x(l,t) \quad [4.5]$$

where $\boldsymbol{W}$ is a N x N unmixing matrix that needs to be estimated to yield the spatially independent components.

4.3 Group ICA

Group ICA is a computational method of identifying independent components in a group of data. Group ICA is a widely used method in resting-state fMRI studies. In order to obtain spatially independent components, data from different scans are temporally concatenated without assuming that the associated temporal response is consistent between sessions/subjects. A schematic diagram of group ICA is presented in Figure 4.1. Group ICA does not assume same temporal response pattern across the population. For each component the final mixing matrix contains the temporal response of all different data sets concatenated into a single column vector. The final reported time course will be the best rank-1 approximation to these different responses.

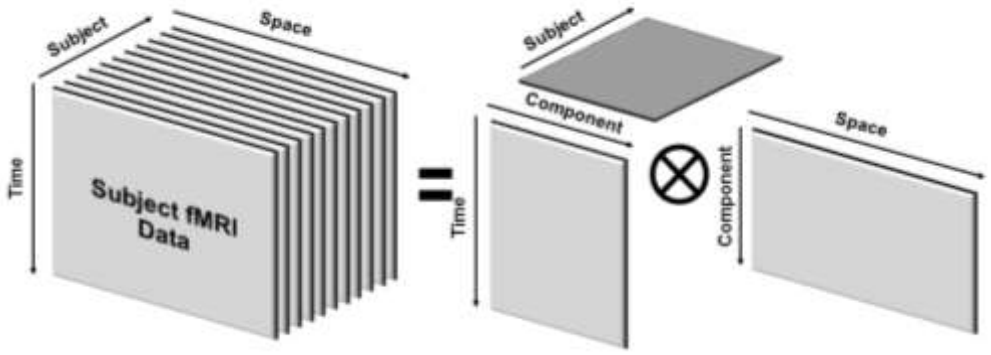

Figure 4.1: Decomposition of spatial group fMRI data into components based on time, space, and subject.

CHAPTER 5

EXPERIMENTAL DESIGN AND DATA ANALYSIS

5.1 Subjects and Neuropsychological Measures

Thirty eight SCI patients are scanned in this study. Participants include 22 paraplegic, 16 tetraplegic, and 23 age-matched healthy control subjects. A comprehensive neurological examination is performed on patients and healthy subjects in order to exclude accompanying neurological disorders of the peripheral and central nervous system. No patient or healthy subject were suffering from a psychiatric disorder or had a history of brain trauma. All subjects are right handed. The study was approved by the local Ethics Committee of Third Hospital of Hebei Medical University. Patients and control subjects gave their written consent to participate in the study. The duration of injury (DOI) for the paraplegic and the tetraplegic subjects ranged from 1-20 months and from 1-51 months respectively. Demographical information of the subjects is presented in Table 6.1.

Neuropsychological tests are used to assess the movement, touch, and pain perceptions of the two SCI groups for both of the left and right limbs. The level and extent of the effects of SCI (motor and sensory deficit) on the patients are assessed according to the protocol of the American Spinal Injury Association (ASIA, 2002). The ASIA scoring system allows to perform a semi-quantitative assessment of the neurological deficits (maximum of motor scores is 100; maximum of sensory scores for each light touch and pin prick sensation is 112). The assessments of motor and sensory scores of the upper and lower limbs describe the extent of SCI and the sensorimotor deficits. All patients suffered a complete traumatic paraplegia or tetraplegia and were in a

stable–chronic clinical condition.

5.2 Imaging Parameter

A high resolution structural image is acquired using magnetization-prepared rapid gradient echo sequence (MPRAGE). The imaging parameters for MPRAGE are as follows - FOV = 240 mm, 512x512 matrix, TR = 2300 ms, TE = 2.91 ms, flip angle = 90°. The whole brain is imaged in an axial configuration where 176 slices are collected and each slice is 1mm thick. The functional images are acquired using echo planer imaging sequence (EPI). The imaging parameters for EPI are FOV = 240 mm, 64x64 matrix, TR = 2000 ms, TE = 27 ms, and flip angle = 90°. The whole brain is imaged in an axial configuration where 20 slices are collected and each slice is 6 mm thick. The resolution is 3.75 mm x 3.75 mm x 6 mm for all functional scans. During the scans the subjects are asked to remain motionless and avoid falling asleep. A total of 195 volumes are collected over a period of 390 seconds during the scan.

5.3 Data Processing

The first 5 volumes are discarded to allow the MR signal to reach equilibrium. The remaining190 volumes are corrected for motion and intra-volume acquisition time offset between the slices using AFNI. Using FSL tools, the corrected fMRI data are spatially smoothed by a Gaussian kernel with 8.25 mm full-width at half-maximum, and temporally filtered with a band-pass filter of 0.01-0.1 Hz in order to reduce the effects of low-frequency drift and high-frequency physiological noise. Legendre polynomials of up to the second order are removed from the processed fMRI data using AFNI in order to

exclude artificial trends. Then all functional images are normalized into the Montreal Neurological Institute space using an optimum 12-parameter affine transformation and nonlinear deformations, and then resampled to 3-mm isotropic voxels.

5.4 Image Analysis

ICA is performed on the preprocessed functional data in two ways. In the first approach (Figure 5.1A), functional data of all of the subjects are temporally concatenated, and then decomposed into 18 independent components using Multivariate Exploratory Linear Optimized Decomposition into Independent Components (MELODIC). The eight resting-state networks estimated using MELODIC are visually identified by comparing with previously defined maps (Beckmann et al., 2005; Smith et al., 2009). Group-ICA spatial maps are back-projected for each subject's fMRI dataset in order to estimate subject-specific temporal components and associated spatial maps using the dual regression technique (Filippini et al., 2009; Zuo et al., 2010).

Dual regression analysis involves two general linear models (GLM) using preprocessed data for individual subjects as a dependent variable. In the first GLM, by using the 18 group ICA component maps as a set of spatial regressors the temporal dynamics associated with each group ICA map are calculated which yielded 18 time-series, each consisting of 190 time-points, for each subject. In the second GLM, the 18 time-series for each subject are used as a set of temporal regressors which yielded subject-specific component maps for each component. The value assigned to a particular voxel in a component map represents a measure of probability that the independent component includes that voxel. Physiologically, the value represents the probability of

whether the voxel is a part of the brain network. Hence, the value assigned to the voxel is a measure of network strength, and is referred as network strength in this study, For each group ICA component, AFNI is used to perform voxel-wise one way Analysis of Variance (ANOVA) in order to asses any difference among the three groups of network strength maps obtained from the three subject groups. Finally, for each ICA component, the probability maps representing difference among the three groups are False Discovery Rate (FDR) corrected using AFNI.

It is imperative that FDR correction be applied when performing multiple hypotheses testing in order to correct for multiple comparisons. FDR modulates the expected number of incorrectly rejected null hypotheses out of the total number of testing, which often referred to as type I error. Type I error can be defined to the error occurs when the null hypothesis is rejected while there is no statistical significance. In the study, FDR correction is particularly useful for avoiding mistakenly observed difference among the three groups.

In the second approach (Figure 5.1B), the functional data is divided into three groups – control, paraplegic, and tetraplegic. Functional data in each group is temporally concatenated, and then decomposed using MELODIC into 17, 25, and 21 independent components, respectively. When studying the differences among pathologies and healthy characteristics, the hypothesis is that some difference exists among the groups. ICA is a statistical approach. Hence, if there are differences among the corresponding independent components for each group, the difference may not be identifiable because of the statistics of the study population as opposed to that of the sample populations corresponding to each group. Therefore, it can be useful to perform ICA on each group

separately.

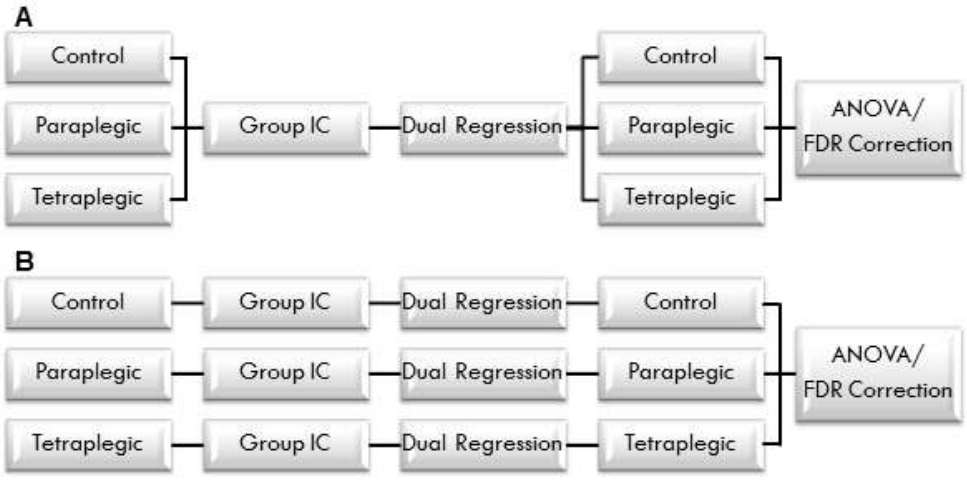

Figure 5.1: A schematic diagram used to depict the two approaches used in the study. (A) The first approach is depicted where the group ICA is performed on the study population, then back-projected to individual subject-data which was then divided into three study groups, and then ANOVA was performed. (B) The second approach is depicted where the group ICA is performed separately on each study group, then back-projected to individual subject-data, and then ANOVA was performed.

An ambiguity of ICA is that the independent components are not necessarily ordered. As shown in Equations 4.1 and 4.2, observed signals are modeled to be weighted sum of its independent components. As a result, when ICA is performed on the three groups separately, there is no direct correspondence between the unraveled independent components. However, it is possible to correlate the independent components by calculating the correlation value between a pair of spatial maps. In this study, the sensorimotor network as reported in resting-state networks is, first, computationally and, then, visually identified from each of the three ICA results. A mask for the sensorimotor network is generated which encompasses the brain regions which showed statistical significance for the sensorimotor component yielded from all of the three ICA results. This mask is used, throughout, the rest of the analysis to avoid the discovery of any non-

overlapping region in the brain. Similar to the first approach, subject-specific temporal and spatial components were estimated using the dual regression technique. ANOVA was performed on the three groups in order to asses any difference in network strength. Finally, for each ICA component, the probability maps representing difference among the three groups and the ICA maps are FDR corrected.

5.5 Network Strength and Neuropsychological Measures

For each ICA component, the back projected spatial maps yielded by dual regression represents the subject-level network strength of the brain network corresponding to each of the ICA component. For the two SCI groups – paraplegic and tetraplegic, Spearman correlation coefficients are calculated between the neuropsychological measurements and the mean network strength of the regions that exhibit group difference.

CHAPTER 6

RESULTS

6.1 Neuropsychological Performance

Table 6.1 represents the neurospsychological performance of the two patient populations. The movement score for the paraplegic group was 27.1±6 whereas for tetraplegic group it was 14.6±12.8. The light touch score for paraplegic and tetraplegic groups were 38.1±9 and 26±17.9, respectively. The pain score for the two groups were 37.2±7.9 and 22.7±16.9, respectively. As shown in Table 1, the paraplegic group scored significantly higher ($p<0.01$) than the tetraplegic group in the three behavioral tests.

Table 6.1: Demographical information of the three groups. Three *Neuropsychological* measurements were made on the two SCI groups. Averages of the contralateral scores were taken for each subject for each *Neuropsychological* measurement. Significant differences ($p<0.05$) in *Neuropsychological* scores were observed for the two SCI groups.

	Control	Paraplegic	Tetraplegic	p value
Demographic Data				
N	23	22	16	
Age (years)	33.5±8.3	35±10	39.9±10.4	
Men:Women	11:12	15:1	17:5	
DOI (months)		1 – 20	1-51	
Neuropsychological Measures				
Movement Score[c]		27.1±6	14.6±12.8	0.0004
Touch Score[c]		38.1±9	26±17.9	0.014
Pain Score[c]		37.2±7.9	22.7±16.9	0.002

DOI = Duration of Injury; [a]three groups were compared using one way ANOVA, [b]two patients groups were compared using unpaired t-test; [c]average of left and right scores;

6.2 Resting-state Functional Networks

Eight major resting-state networks (Figure 6.1) – visual, lateral occipital, auditory, sensory motor, default mode, executive control and left and right lateralized fronto-parietal - were visually identified by comparing the 18 ICA components yielded by MELODIC with previous reports (Beckmann et al., 2005; Damoiseaux and Greicius, 2009). The right lateralized fronto-lateral network (RLFL) and the default mode network

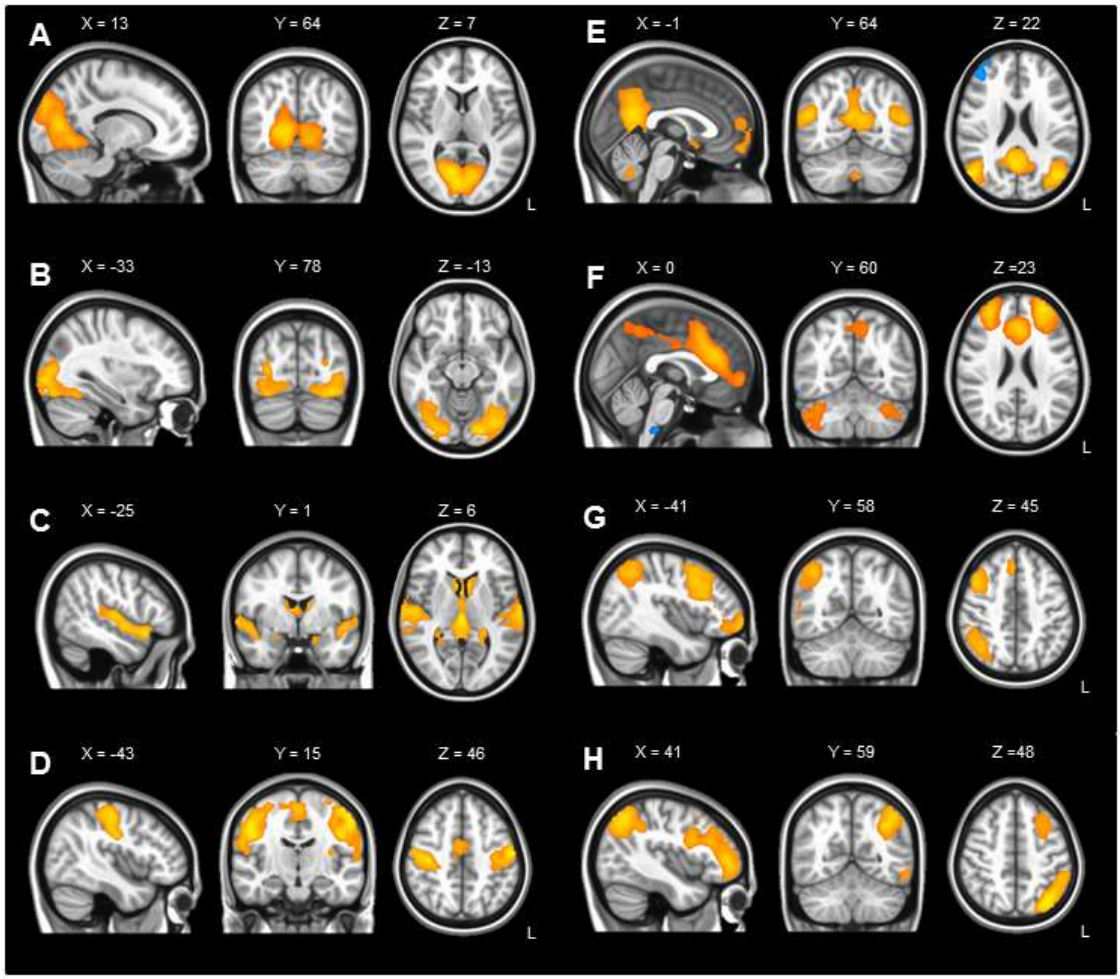

Figure 6.1: Eight group spatially independent component analysis component maps from 65 subjects: (A) primary visual, (B) lateral occipital cortex (LOC), (C) auditory, (D) sensory-motor, (E) the ‘‘default mode’’ network (DMN), (F) executive control, and (G, H) two right- and left-lateralized fronto-parietal networks. All images have been coregistered into the space of MNI template. The coordinates refer to millimeter distances from the anterior commissure and images are shown in radiological convention. Z value of 3.09 is used for thresholding the component maps.

(DMN) showed significant differences among the three groups. Two regions in the RLFL showed significant difference. Using the Talairch and Tournoux atlas the two regions were identified to be in the right inferior frontal gyrus (RIFG) near right precentral gyrus (X = -60, Y = -5, Z = 25, Figure 6.2A) and the right cerebral white (RCW) matter near the right cingulate gyrus (X = -23, Y = 13, Z = 32, Figure 6.2C), respectively. Unpaired t-tests between pairs of the three groups indicated that the network strength within RIFG of tetraplegic group was significantly lower than that of the control

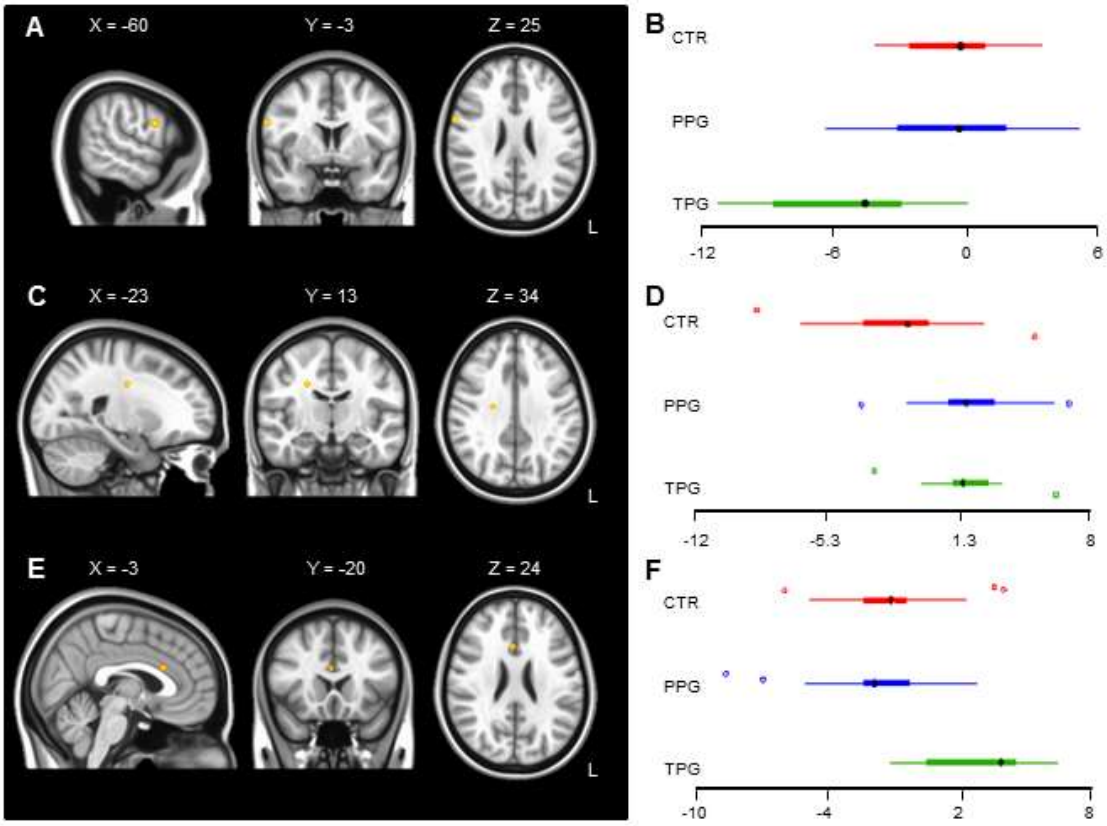

Figure 6.2: (A) Significant group difference ($p<0.05$, FDR Corrected) for the RLFL network in the RIFG near right precentral gyrus, and right Brodmann areas 9 and 44 (X= -60, Y= -5, Z = 25). (C) Significant group difference ($p<0.05$, FDR Corrected) for the RLFL network in the RCW near right cingulate gyrus (X= -23, Y= -13, Z = 32). (E) Significant group difference ($p<0.05$, FDR Corrected) for the DMN network in the ACC near right Brodmann areas 24 and 33 (X= -4, Y= -20, Z = 23). (B,D) Box and whisker plot of the mean network strength of RIFG and RCW in the RLFL network for the three subject groups respectively. (F) Box and whisker plot of the mean network strength of right ACC in the DMN network for the three subject groups respectively.

and the paraplegic groups (Figure 6.2B). Unpaired t-tests between pairs of the three groups also indicated that the network strength in the RCW was significantly lower for the control group as opposed to the two SCI groups (Figure 6.2D). The right anterior cingulate cortex (ACC) near Brodmann areas 24 and 33 (X = -4, Y = -20, Z = 23, Figure 6.2E) in the DMN was found to be significantly different among the three groups. Unpaired t-tests between pairs of the three groups indicated that the network strength in ACC was significantly higher for the tetraplegic group compared to that of the control and the paraplegic groups (Figure 6.2F).

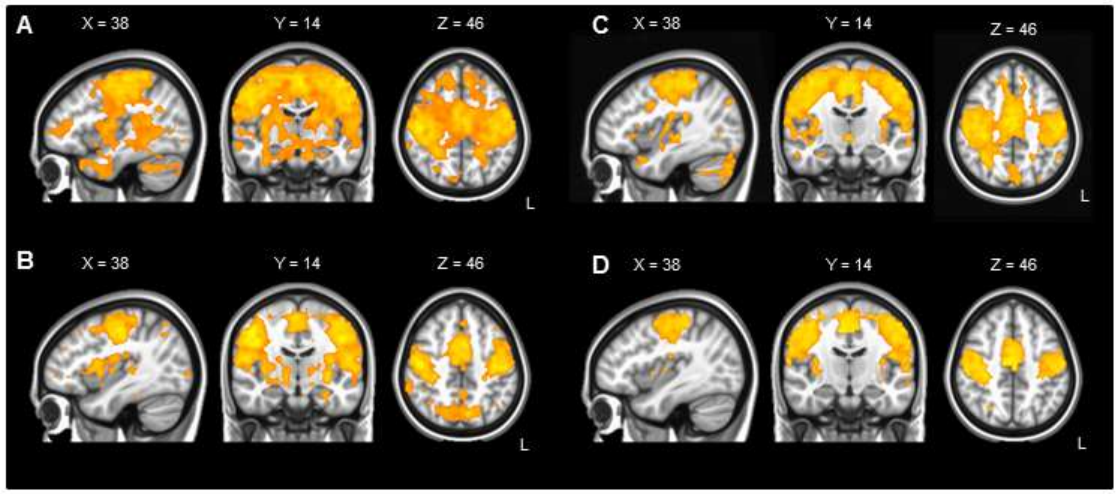

Figure 6.3: Sensorymotor component yielded from independent component analysis component of the three groups – (A) control, (B) paraplegic, (C) tetraplegic. (D) A mask of the sensory motor component defined by the regions that were included in all three sensorymotor component as shown in (A), (B), and (C). The coordinates refer to millimeter distances from the anterior commissure and images are shown in radiological convention. All maps were corrected for FDR (<0.05) and thresholded for $p<0.05$.

In the second approach, ICA is performed on three groups of data separately. A spatial correlation between the independent components is calculate to find corresponding ICs from the three ICA results. The sensorymotor networks obtained from the three ICAs are illustrated in Figure 6.3. Since the spatial maps of the three ICs encompassed varying regions, in the study the focus is placed on the brain regions that

were significant in all three spatial maps. The overlapping brain-map is shown in Figure 6.3D. Four clusters are identified in the difference map, which are illustrated in Figure 6.4A. The clusters are named as cluster1(green), cluster2(light green), cluster3(orange), and cluster4(red). Cluster1 is located in the left postcentral gyrus near left Brodmann area 3 (X= -39, Y= -36, Z = 51). Cluster2 is located in the right precuneus near right Brodmann area 7 (X= -18, Y= -63, Z = 60). Cluster3 is located in the right precuneus

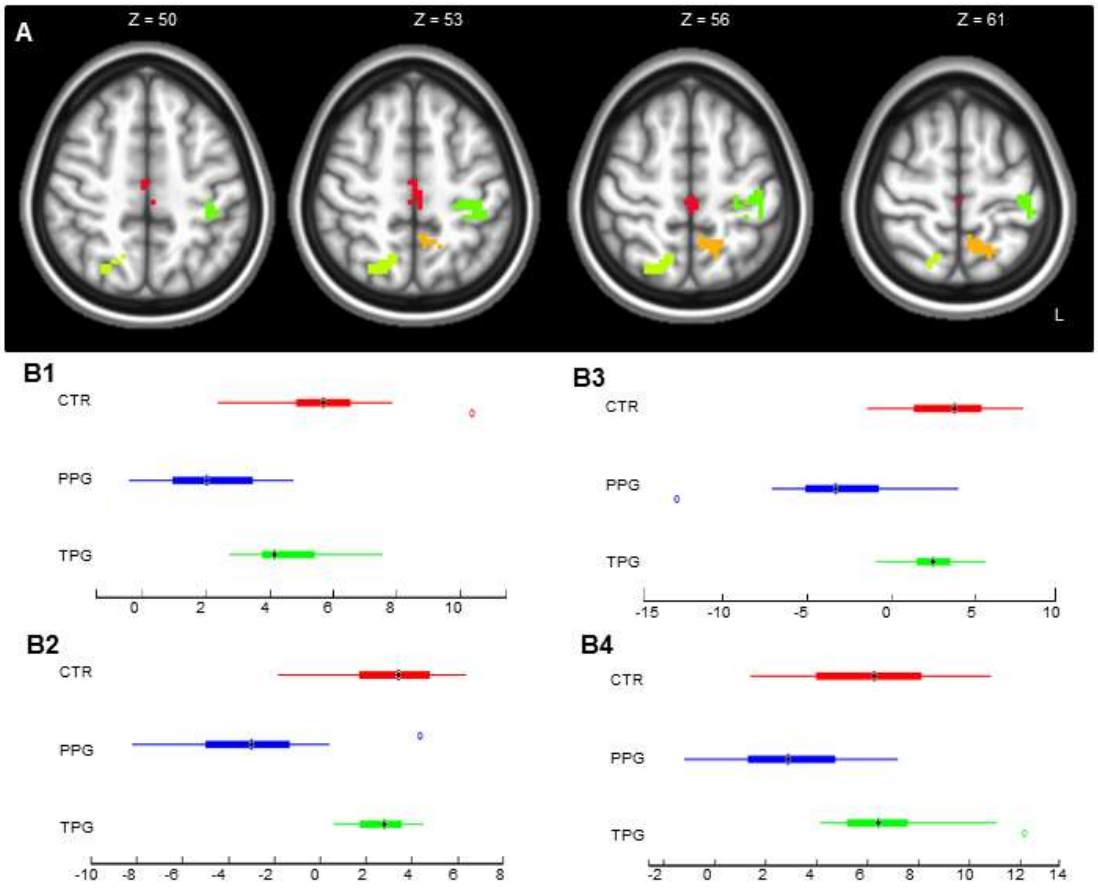

Figure 6.4: (A) Significant group difference ($p<0.05$, FDR Corrected) for the sensorymotor network. Four clusters were identified that showed significant difference among the three groups. Cluster-1 (green) is located in the left postcentral gyrus near left Brodmann area 3 (X= -39, Y= -36, Z = 51). Cluster-2 (light green) is located in the right precuneus near right Brodmann area 7 (X= -18, Y= -63, Z = 60). Cluster-3 (orange) is located in the right precuneus near left Brodmann area 7 (X=15, Y= 54, Z = 60). Cluster-4 (red) is located in the medial frontal gyrus near Brodmann area 6 (X= 0, Y= 27, Z = 57).

near left Brodmann area 7 (X=15, Y= 54, Z = 60). Cluster4 is located in the medial frontal gyrus near Brodmann area 6 (X= 0, Y= 27, Z = 57). The three samples of mean network strength of the three groups, for each of the four clusters, are represented in the box-and-whiskers plot in Figure 6.4B. Unpaired t-tests between pairs of the three groups indicated that the network strength in all of the four clusters was lower for the paraplegic group as opposed to the control and the tetraplegic groups (Figure 6.4B). Cluster1, located in the left-postcentral gyrus had higher network strength for the control group as opposed to both of the patient groups (Figure 6.4B1).

6.3 Behavioral Score and Network Strength

Figure 6.5 represents the relationship between neuropsychological performance of paraplegic and tetraplegic subjects with the RLFL network strength of RIFG region which showed difference among the groups. Linear trends for the sensory scores suggest that for paraplegic subjects the score increases with increasingly positive network strength whereas for tetraplegic patients the score increases with increasingly negative

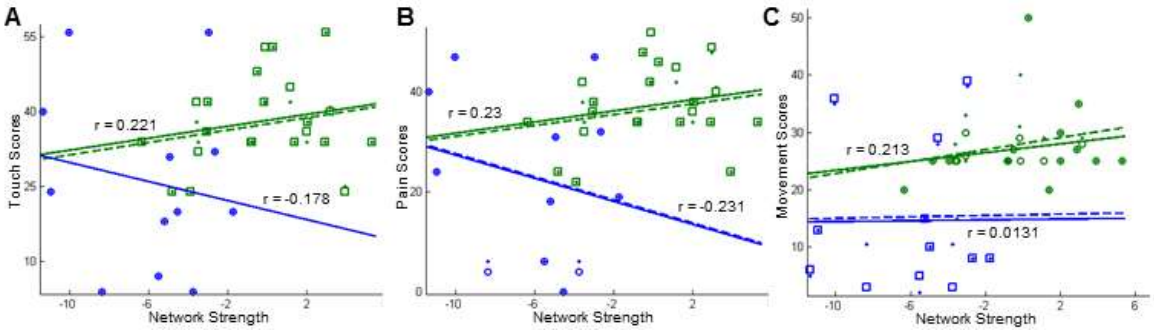

Figure 6.5: Relationship of network strength of RIFG in the RLFL network with the neurophysiological scores. Green and blue represents the paraplegic and the tetraplegic groups respectively. The neurophysiological scores for the right and the left sides are represented by dots and circles/squares respectively. A, B, and C represents the neurophysiological scores for touch, pain, and movement respectively.

network strength (Figure 6.5A,B). Linear trends for the movement score suggest that with increasingly positive network strength, the performance of movement improves for both of the patient populations (Figure 6.5C).

Figure 6.6 represents the relationship between neuropsychological performance of paraplegic and tetraplegic subjects with the RLFL network strength of RCW region which showed difference among the groups. Linear trends for the sensory scores suggest that for paraplegic subjects the score increases with increasingly negative network strength whereas for tetraplegic patients the score increases with increasingly positive network strength (Figure 6.6A,B). Linear trends for the movement score suggest that with increasingly positive network strength, the performance of movement improves for both of the SCI patient populations (Figure 6.6C).

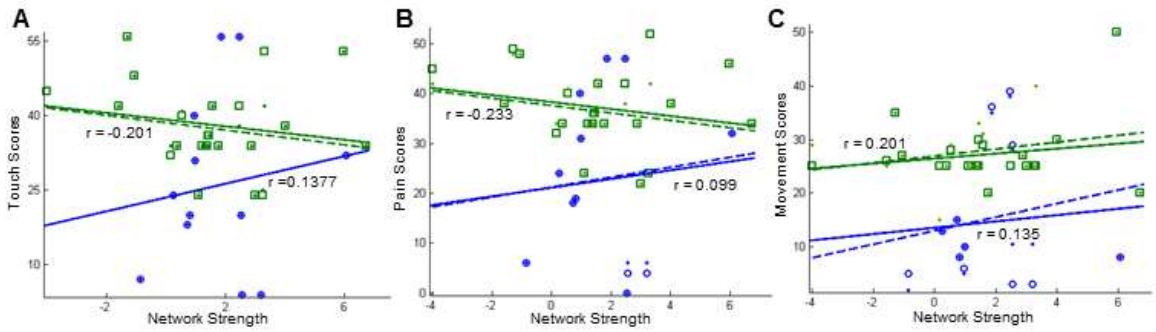

Figure 6.6: Relationship of network strength of RCW in the RLFL network with the neurophysiological scores. Green and blue represents the paraplegic and the tetraplegic groups respectively. The neurophysiological scores for the right and the left sides are represented by dots and circles/squares respectively. A, B, and C represents the neurophysiological scores for touch, pain, and movement respectively.

Figure 6.7 represents the relationship between neuropsychological performance of paraplegic and tetraplegic subjects with the DMN network strength of ACC region which showed difference among the groups. Linear trends for the sensory scores suggest that for paraplegic subjects the score increases with increasingly negative network strength

whereas for tetraplegic patients the score increases with increasingly positive network strength (Figure 6.7A,B). Linear trends for the movement score suggest that with increasingly positive network strength, the performance of movement improves for tetraplegic patients and deteriorates for paraplegic patients (Figure 6.7C).

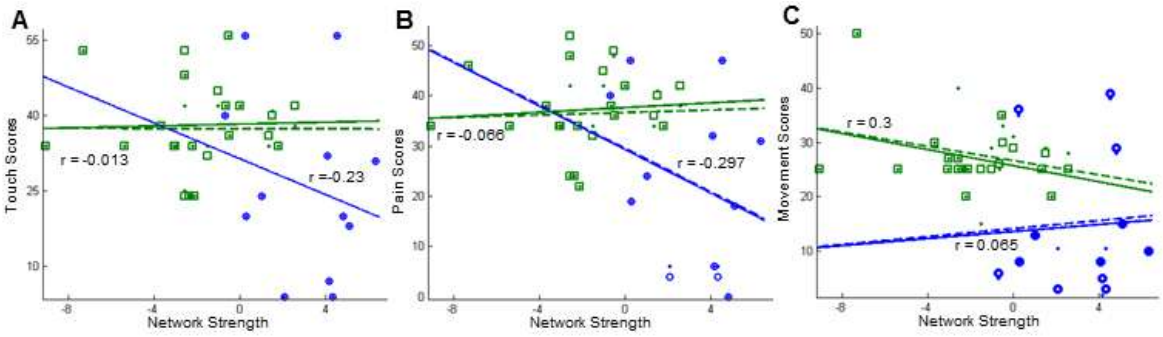

Figure 6.7: Relationship of network strength of right ACC in the DMN network with the neurophysiological scores. Green and blue represents the paraplegic and the tetraplegic groups respectively. The neurophysiological scores for the right and the left sides are represented by dots and circles/squares respectively. A, B, and C represents the neurophysiological scores for touch, pain, and movement respectively.

Figure 6.8 represents the relationship between neuropsychological performance of paraplegic and tetraplegic subjects with the sensormotor network strength of left postcentral gyrus near left Brodmann Area 3, which showed difference among the groups. Linear trends for the sensory scores suggest that for both, paraplegic and tetraplegic, subjects the score increases with increasingly positive network strength (Figure 6.8A,B). Linear trends for the movement score suggest that with increasingly positive network strength, the performance of movement improves for the paraplegic subjects whereas deteriorate for the tetraplegic patient populations (Figure 6.8C). It can be also noted that the correlation r-value of the sensory scores with the network strength is much higher than that of the movement score.

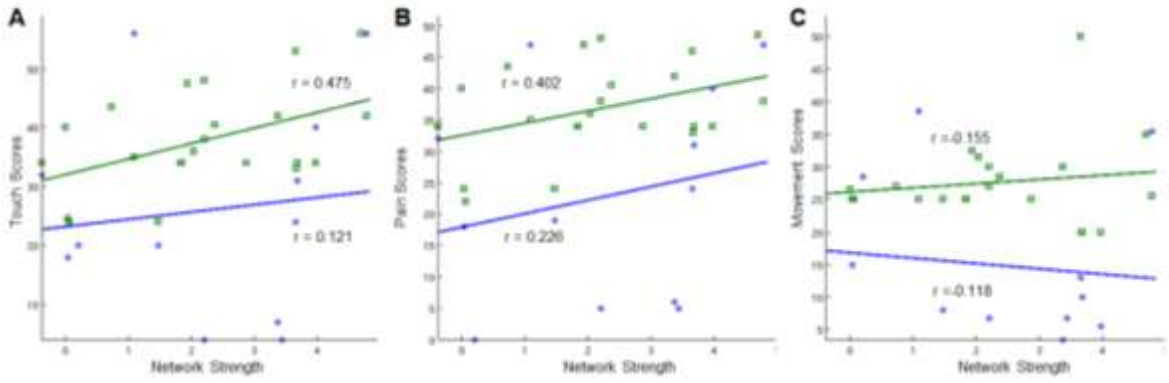

Figure 6.8: Relationship of network strength of left postcentral gyrus in the sensorymotor network with the neurophysiological scores. Green and blue represents the paraplegic and the tetraplegic groups respectively. A, B, and C represents the neurophysiological scores for touch, pain, and movement respectively.

Figure 6.9 represents the relationship between neuropsychological performance of paraplegic and tetraplegic subjects with the sensormotor network strength of right precuneus near right Brodmann Area 7, which showed difference among the groups. Linear trends for the both, sensory and movement, scores suggest that for both, paraplegic and tetraplegic, subjects the score increases with decreasing network strength (Figure 6.9). It can be also noted that the correlation r-value of the paraplegic motor score with the network strength is much higher than that of the tetraplegic score.

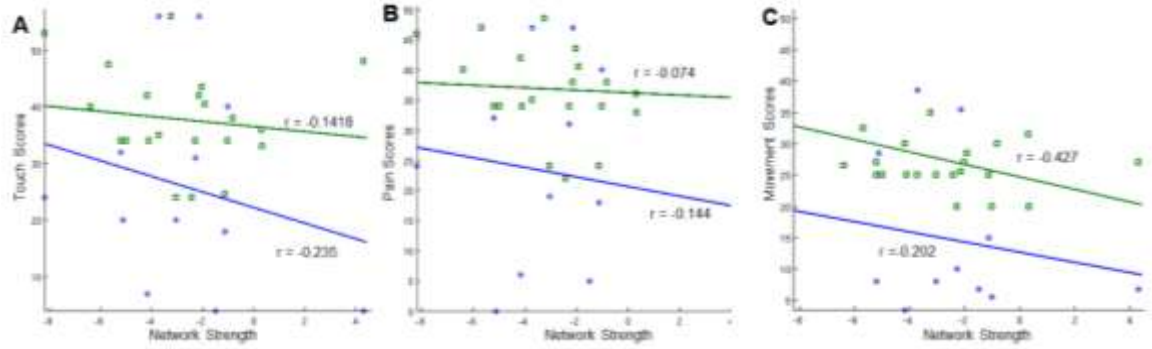

Figure 6.9: Relationship of network strength of left precuneus in the sensorymotor network with the neurophysiological scores. Green and blue represents the paraplegic and the tetraplegic groups respectively. A, B, and C represents the neurophysiological scores for touch, pain, and movement respectively.

Figure 6.10 represents the relationship between neuropsychological performance of paraplegic and tetraplegic subjects with the sensormotor network strength of left precuneus near left Brodmann Area 7, which showed difference among the groups. Linear trends for the both, sensory and movement, scores suggest that for both, paraplegic and tetraplegic, subjects the score increases with decreasing network strength (Figure 6.10). It can be also noted that the correlation r-values of the paraplegic sensory score with the network strength are nominal. The correlation r-values of the tetraplegic motor as well as sensory score with the network strength are higher than that of the paraplegic group (Figure 6.10).

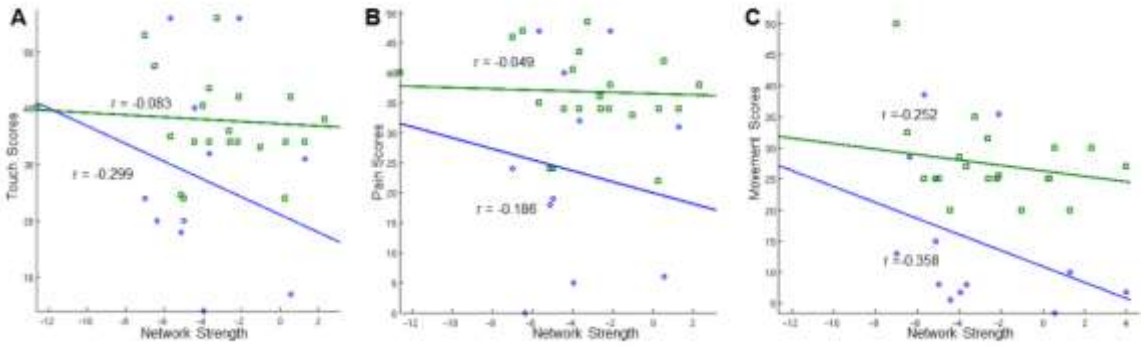

Figure 6.10: Relationship of network strength of right precuneus in the sensorymotor network with the neurophysiological scores. Green and blue represents the paraplegic and the tetraplegic groups respectively. A, B, and C represents the neurophysiological scores for touch, pain, and movement respectively.

Figure 6.11 represents the relationship between neuropsychological performance of paraplegic and tetraplegic subjects with the sensormotor network strength of the medial frontal gyri near Brodmann Area 6, which showed difference among the groups. Linear trends for the sensory scores suggest that for tetraplegic subjects the score increases with decreasing network strength (Figure 6.11A,B) whereas strong correlation is absent between the paraplegic sensory scores and the network strength. It can be also

noted that the correlation r-values of the paraplegic sensory score with the network strength are nominal. The correlation r-values of the motor score of the two groups with the network strength is negative and nominal as well (Figure 6.11C).

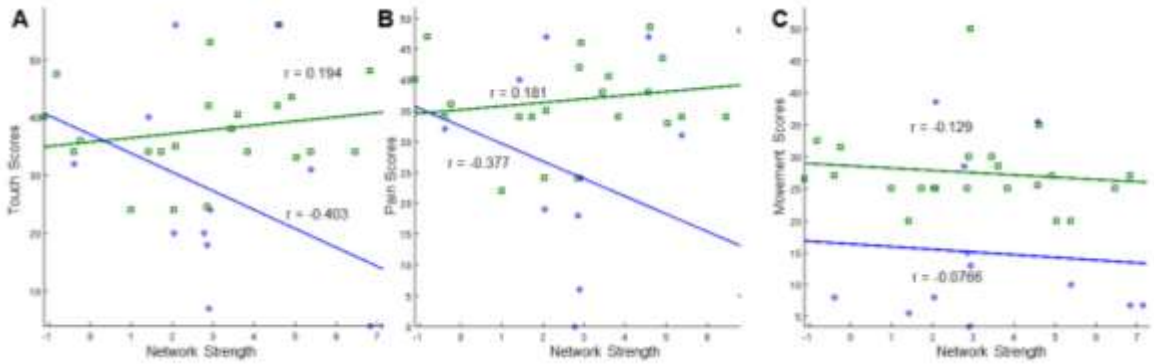

Figure 6.11: Relationship of network strength of medial frontl gyri in the sensorymotor network with the neurophysiological scores. Green and blue represents the paraplegic and the tetraplegic groups respectively. A, B, and C represents the neurophysiological scores for touch, pain, and movement respectively.

Table 6.2: Correlation values for the network strength and neurological score.

	Touch		*Pain*		*Motion*	
	Paraplegic	Tetraplegic	Paraplegic	Tetraplegic	Paraplegic	Tetraplegic
RLFL1	0.221	-0.178	0.23	-0.231	0.213	0.013
RLFL2	-0.201	0.137	-0.233	0.099	0.201	0.135
DMN	0.013	-0.23	0.066	-0.297	-0.3	0.055
SM1	0.475	0.121	0.402	0.226	0.155	-0.118
SM2	-0.142	-0.235	-0.074	-0.144	-0.427	-0.202
SM3	-0.083	-0.299	-0.049	-0.186	-0.252	-0.358
SM4	0.194	-0.403	0.181	-0.377	-0.129	-0.0766

RLFL1 = Region of difference in right precentral gyrus near BA9 and BA44 from RLFL network.

RLFL2 = Region of difference in RCW from RLFL network.

DMN = Region of difference in right ACC from DMN.

SM1 = Region of difference in left postcentral gyrus near BA3 from sensorymotor network.

SM2 = Region of difference in right precuneus near BA7 from sensorymotor network.

SM3 = Region of difference in left precuneus near BA7 from sensorymotor network.

SM4 = Region of difference in medial frontal gyrus near BA6from sensorymotor network.

Table 6.2 summerizes the correlation values of the network strength with the neurological assessment scores for the two subject group. Significant correlation was observed in six cases and similar trends were observed for lower correlation values.

CHAPTER 7

DISCUSSION AND CONCLUSIONS

The present study uses resting state fMRI analysis in order to delineate altered functional changes in brain networks after SCI. Although preliminary in nature, a number of observations are made in this study. This study demonstrates altered resting state brain connectivity in patients with SCI. Furthermore, distinct differences between the two SCI groups suggest alterations in functional connectivity. Finally, significant correlation between network strength and clinical measures in the SCI patients is observed. By using ICA, a number of different networks - primary visual, lateral occipital cortex (LOC), auditory, sensory-motor, the ‘‘default mode’’ network (DMN), executive control, and two right- and left-lateralized fronto-parietal networks – were revealed. Distinct differences were found among the three groups for three of the neural networks.

It is observed that the right Brodmann areas 44 (BA44) and 9 (BA9), near RIFG and right precentral gyrus, of the tetraplegic group have significantly lower network strength than that of the control and the paraplegic groups. RIFG has been typically associated with go/no-go tasks (Aron et al., 2004). In such a task, the participant has to inhibit a prepotent response; for instance stop pressing a button when a red signal appears. The same region has been associated with risk aversion; a study found that higher risk aversion correlated with higher activity in the IFG (Christopoulos et al., 2009). This might be explained as an inhibition signal to accept a risky option. Disruption of activity in this area with Transcranial Magnetic Stimulation (TMS) or Direct Current Stimulation (tDCS) leads to changes in attitude towards risks, as behaviorally

demonstrated by choices over risky outcomes (Knoch et al., 2006; Fecteau et al., 2007). The lateral prefrontal region near BA 9 is typically involved in working memory tasks, in tasks of sustained attention and (bilaterally) in tasks demanding problem solving (Cabeza and Nyberg, 2000). Hence, the weaker network strength in the tetraplegic group suggests an impairment of higher level cognitive and executive functions after SCI. Precentral gyrus works in association with the planning and execution of movements. Interestingly, no significant difference was seen between the healthy control group and the paraplegic group. Since the upper-body movement functions are mostly intact in the paraplegic patients, the weaker network strength in the tetraplegic group may be associated with the impairment of most limb movement functions.

The second difference is observed in the right cerebral white (RCW) matter near the right cingulate gyrus. The network strength in the RCW is significantly lower for the control group as opposed to the two SCI groups. White matter, long thought to be composed of passive tissues, actively affects how the learning process and other brain functions. While gray matter is associated with the cognitive processes in the brain, white matter is associated with the modulation of signals that neurons in gray matter generate with rest of the brain and, thereby, coordinates different brain regions (Fields et al, 2008). Unlike gray matter, which peaks its development in the twenties, the white matter continues to develop and peaks at middle age (Sowell et al, 2003). It should be noted that the claim has been disputed in recent years.

Diffusion tensor imaging (DTI) has the potential to non-invasively provide information about altered connectivity between different brain regions in response to SCI. DTI utilizes the directionality of water diffusion in tissue. The fiber structure within the

white matter results in higher diffusion anisotropy relative to gray matter that is typically made of cell bodies with relatively little preference for orientation. It is generally believed that the directionality or anisotropy in diffusion reflects the integrity of tissue microstructural reorganization. Diffusion anisotropy is determined both by the axonal structure and the condition of myelin (Beaulieu, 2002; Gulani et al., 2001). Both, damage to axonal structure and demyelination, affect the observed anisotropy. Therefore, diffusion anisotropy can provide valuable information about altered white matter structure. The anisotropy or directionality of diffusion can be quantified by scalar quantities such as fractional anisotropy (FA).

The results also show that the right anterior cingulate cortex (ACC) near Brodmann areas 24 and 33 in the DMN was significantly different among the three groups. The network strength in ACC was significantly higher for the tetraplegic group as opposed to that of the control and the paraplegic groups. The DMN has received increasing attention in recent years. DMN reflects an ensemble of cortical regions typically deactivated during demanding cognitive tasks in fMRI studies (Raichle et al., 2001). Using functional connectivity, this network can be conceptualized and studied as a "stand-alone" function or system. Major regions in the DMN include the precuneus, anterior cingulate gyri, and posterior cingulate gyri. Additional regions include the superior and middle temporal as well as frontal gyri, the inferior parietal lobule and parahippocampal gyrus. Briefly, these regions are thought to be related to recognition, social communication, working memory, and some auditory demands. The activation of this network has been reported, in numerous studies, to increase during resting state and suspend during specific goal-directed behaviors (Garrity et al., 2007; Raichle et al.,

2001).

Ventral anterior cingulate (Brodmann area 24) relate to many areas in the brain. ACC receives, primarily, its afferent axons from the intralaminar and midline thalamic nuclei. The anterior nuclei receive mammillo-thalamic afferences. The mammillary neurons receive axons from the subiculum. The overall network contains a portion of the Papez circuit. The ACC sends axons to the anterior nucleus and through the cingulum to other Broca's limbic areas. The ACC is involved in error and conflict detection processes, such as in the go/no-go task. Our SCI affected right ACC corresponds to the "default mode network" that participates in episodic memory (Buckner et al., 2005) and became known for its task-related deactivations across fMRI studies (Fox et al., 2005; Fransson, 2005; Greicius et al., 2003). Thus, it seems unlikely that this local increase in connectivity is due to loss of association fibers or lower acetylcholine levels. A possible, but at this stage highly speculative, explanation could be that the connectivity reflects a compensation mechanism in a relatively healthy part of the network.

A PET study (Roelcke et al., 1997) at rest found relatively higher CMRGlu in the frontal lobe of patients with spinal cord injury, which bilaterally comprised most of the supplementary motor area, caudally extended into the anterior cingulate (Brodmann area 24), and more laterally towards the motor cortex. These brain regions are involved in movement preparation and execution, as well as in intentional aspects of motor tasks, particularly in the supplementary motor cortex, putamen, and anterior cingulated (Brodmann area 32). Relatively increased CMRGlu in the above mentioned regions could be attributed to hyperactivity of neurons which originate within, or which project to these regions. It may reflect a relative disinhibition, secondary to reduction or loss of afferent

impulses, which mediates synaptic reorganization. Our results may be explained using the viewpoint.

A study using rest SPECT found significantly reduced blood flow rates in some of the movement-cortical and subcortical areas following SCI. The areas of significantly reduced rCBF consisted of bilateral anterior cingulate gyrus in the paraplegic patient group and left anterior cingulate gyrus in tetraplegic patient group. It may be possible to determine the disrupted regional blood flow areas because of the loss of function resulting from the cell atrophy (Çermika et al., 2006). Disinhibition and cell atrophy were the results accompanying SCI. The contrary results may relate to the duration of SCI.

A DTI study (Wrigley et al., 2009) found that SCI results in significant changes in the anatomy of the medial prefrontal and anterior cingulate cortices. These brain regions are known to be critical for the processing of emotional relevant information and in modulating states involved with attention. It has been shown by Damasio et. al that the peripheral arousal levels may influence the emotional state, and it has been suggested that the decoupling of the brain from the body, as it happens following SCI, may modify emotional experiences (Damasio, 1994). Indeed, a recent fMRI investigation has revealed reduced activity in the subgenual anterior cingulated cortex during emotional processing in SCI subjects (Nicotra et al., 2006). It may be that changes in the anatomy of the prefrontal/anterior cingulate cortices are reflected in changes in emotional processing in SCI subjects, although the precise nature of these anatomical changes cannot be determined using MRI techniques. Our results may reflect the modulating compensation to emotional processing in SCI.

In this study, four regions show significant differences among the three groups for the sensorimotor network. The first region, Cluster1, is located in the left postcentral gyrus which is an important landmark in the brain. The primary somatosensory cortex includes postcentral gyrus. It has been found to be the main area receptive to the sense of touch. Brodmann area 3 (BA3) is referred to as "primary somatosensory cortex" because it receives the most of the thalamocortical projections from the sensory inputs (Reed et. al, 2008). BA 3 receives dense inputs from the pulvinar nucleus of the thalamus. Also, the neurons located in BA3 are highly responsive to somatosensory stimuli, however, not to other stimuli. Furthermore, lesions in BA3 can impair somatic sensation while electrical stimulation of BA3 can evoke somatic sensory activation. BA3 has also been associated with proprioception. In this study, it is found that the left-postcentral gyrus near BA3 of the paraplegic group has lower connectivity strength than that of the control group. Since all of the subjects in the study were right-handed, left hemisphere is the dominant in the brain. After SCI, paraplegic patients receive sensory inputs from the upper two limbs and most of the torso, however, does not receive any sensory input from the lower limbs. Hence, the reduction in network strength may be correlated to the reduction of input sensory signal. In addition, the network strength in the postcentral gyrus of the tetraplegic group is significantly less than that of the healthy control group. Tetraplegic subjects receive little to nothing from the four limbs and most of the body. The less sensory signal received by tetraplegic subjects may explain the reduction of network strength in the postcentral gyrus. Interestingly, the tetraplegic group appears to have higher network strength than that of the paraplegic group.

The second and the third regions, Cluster2 and Cluster3, are located in the right and left precuneus near Brodmann area 7 (BA7), respectively. The precuneus is involved with visual-spatial processing, episodic memory, and different aspects of consciousness. The precuneus is situated between the two somatosensory cortices and forward of the visual cortex. Although, connections have not been reported between the precuneus and the primary motor cortex, there are connections between the precuneus and the sensorimotor cortex as well as the primary visual cortex. It has been suggested that the precuneus is involved in directing attention in space when both, an individual makes movements and when imagining or preparing to make a movement (Cavanna and Trimble, 2006; Kawashima et. al, 1995). The motor coordination required for shifting attention to spatial locations has also been attributed to the precuneus (Wenderoth et. al, 2005). While the premotor regions engage in the mental operation of imagining a motion, the precuneus is suggested to be aiding the monitoring of that operation by incorporating visual images (Oshio et. al, 2010). This study found that the network strength in the precuneus of the paraplegic group is less than that of the healthy control group whereas is unchanged for the tetraplegic group.

Since paraplegic subjects are unable to receive or send signal to the lower limbs, their visual-spatial processing needs to be adjusted which may be done through alterations in the precuneus and/or postcentral gyrus regions of the sensorimotor network (Kim et. al, 2010). It is possible that, as opposed to the paraplegic group, tetraplegic subjects do not receive any sensory input signal and, therefore, it is not only the reduction in the signal received but also an “all or none” system that causes reduction in signal strength. In this case, the “all” and the “none” in the system are analogous to the healthy

control group and the tetraplegic group, respectively. Therefore, for the tetraplegic group, because significantly less amount of sensory input is received by the brain, the reduction in network strength is less than that of the paraplegic group as the system may not have been able to detect the change whereas for the paraplegic group the reduction of sensory input signal is essentially half of that of the healthy control group which may have been easily detected by the system causing more alteration in the functional connectivity. Conversely, the drastic loss of sensory input and motor output in tetraplegic patients may resume a faster compensatory mechanism which may explain the higher network strength in tetraplagic subjects.

The fourth brain regions showing difference for the sensorimotor network is located in the Brodmann area 6 (BA6) near medial frontal gyrus. BA6 is reported to bridge the prefrontal and the primary motor cortices. The caudal portions of BA6 are related to the primary motor cortex, which send extensive corticospinal projections. The rostral portions of BA6 have close connections with the prefrontal cortex, however, lack a direct projection to the spinal cord (Barbas and Pandya, 1987; Luppino et al., 1993; Lu et al., 1994). Neuroimaging studies reported that BA6 is activated during both, demanding motor tasks (Roland et al., 1980; Catalan et al., 1998; Grafton et al., 1998) and various cognitive tasks (Jonides et al., 1993; Mellet et al., 1996; Lamm et al., 2001; Simon et al., 2002; Hanakawa et al., 2003a,b). However, the functions of BA6 for cognition are poorly understood as opposed to those for motor control (Picard and Strick, 2001; Schubotz and von Cramon, 2003).

From the correlation analysis of the neuropsychological assessments with the network strength of the regions that demonstrated difference among the groups, it may be

inferred that there may be some relationship between the network strength in the sensorimotor network and the neuropsychological assessment score. The correlation of both of the sensory scores is high and positive for the paraplegic group with the network strength in the left postcentral gyrus near BA3. Similar trend is visible for the tetraplegic group; however, the correlation values are lower than that of the paraplegic group. As mentioned earlier, postcentral gyrus is associated with proprioception and highly responsive to somatosensory stimuli. Since the network strength in the region for the healthy control group is significantly higher than that of the two SCI patient groups, the positive correlation of network strength and sensory neurological assessment scores further validates the finding. Moreover, the region may be used as a biomarker for the rehabilitation research of SCI patients. The correlation between the motor neurological assessment for the paraplegic group and the network strenght in the right precuneus is negative and high. Similar trend is visible for the tetraplegic group; however, the correlation values are lower than that of the paraplegic group. It was previously mentioned that the precuneus is significant for the visual-spatial processing which is an essential step for any motor movement. It may be inferred from the results that a compensatory mechanism may be present that causes the network strength to increase for increasingly impaired SCI patients. Moreover, all of the subjects are right handed and the right hemisphere is non-dominant which strengthens the claim regarding the compensatory mechanism and plasticity in the brain (Ivaneko et. al 2009; Manning, 2008; Scivoletto et. al, 2007). Hence, there is a negative correlation between network strength and motor assessment score. A similar inference may be drawn for the region showing difference in the right precuneus, except that the correlation value is high for the

tetraplegic group as opposed to that for the paraplegic group. The results suggest that there is a negative and high correlation between the network strength of BA3 near medial frontal gyrus for the tetraplegic group where as it is positive for the paraplegic group. BA3 is associated with demanding motor tasks and cognitive tasks. The more sever impairment of the tetraplegic patients may be attributed to the negative correlation as a result of a compensatory mechanism which increases the network strength more in more impaired paraplegic subjects. Conversely, a positive correlation trend is present between the network strength and the sensory scores; although the correlation values are lower than that for the tetraplegic group.

In conclusion, this study, although preliminary in nature, confirms that a simple resting-state condition may be sufficient to demonstrate widespread changes in functional connectivity in SCI. Analysis of resting state network activity in SCI demonstrated significant changes not only in cortex but also in white matter. Besides involved in movement preparation and execution, the present results demonstrate extra-motor involvement in SCI. The default mode involved has been linked to cognitive processes, consisting of episodic memory, processing of emotional, and performance of motor activity. Hence, RSNs can provide useful clinical or cognitive markers during task-free conditions after SCI.

REFERENCES

1. Alkadhi H, Brugger P, Boendermaker SH, Crelier G, Curt A, Hepp-Reymond MC, Kollias SS. What disconnection tells about motor imagery: evidence from paraplegic patients. Cereb Cortex. 2005;15:131-140.

2. Aron AR, Robbins TW, Poldrack RA. Inhibition and the right inferior frontal cortex. Trends Cogn Sci**.** 2004; 8-4: 170-177.

3. ASIA, 2002. International standards for neurologic classification of spinal cord injury patients. American Spinal Injury Association, Chicago.

4. Barbas H, Pandya DN. Architecture and frontal cortical connections of the premotor cortex (area 6) in the rhesus monkey. J Comp Neurol, 1987; 256: 211-228.

5. Bareyre FM, Kerschensteiner M, Raineteau O, Mettenleiter TC, Weinmann O, Schwab ME.. The injured spinal cord spontaneously forms a new intraspinal circuit in adult rats. Nat Neurosci. 2004; 7:269.

6. Beaulieu C. The basis of anisotropic water diffusion in the nervous system - a technical review. NMR Biomed 2002; 15:435-455.

7. Beaud ML, Schmidlin E, Wannier T, Freund P, Bloch J, Mir A, Schwab ME, Rouiller EM. Anti-Nogo-A antibody treatment does not prevent cell body shrinkage in the motor cortex in adult monkeys subjected to unilateral cervical cord lesion. BMC Neurosci. 2008; 9:5.

8. Beckmann, C.F., DeLuca, M., Devlin, J.T., Smith, S.M.. Investigations into restingstate connectivity using independent component analysis. Philos. Trans. R. Soc. Lond B Biol. Sci. 2005; 360:1001-1013.

9. Biswal B, Yetkin FZ, Haughton VM, Hyde JS. Functional connectivity in the motor cortex of resting human brain using echo-planar MRI. Magnetic resonance in medicine: official journal of the Society of Magnetic Resonance in Medicine/Society of Magnetic Resonance in Medicine. 1995; 34:537-541.

10. Bruehlmeier M, Dietz V, Leenders KL, Roelcke U, Missimer J, Curt A. How does the human brain deal with a spinal cord injury? Eur J Neurosci. 1998;10:3918-3922.

11. Buckner RL, Snyder AZ, Shannon BJ, LaRossa G, Sachs R, Fotenos AF, Sheline YI, Klunk WE, Mathis CA, Morris JC, Mintun MA. Molecular, structural, and functional characterization of Alzheimer's disease: evidence for a relationship between default activity, amyloid, and memory. J Neurosci 2005; 25:7709-7717.

12. Cabeza, R., Nyberg, L., 2000. Imaging cognition II: an empirical review of 275 PET and fMRI studies. J. Cogn Neurosci. 12, 1-47.

13. Calhoun VD, Eichele T, Pearlson G. Functional brain networks in schizophrenia: a review. Front Hum Neurosci. 2009; 3:17.

14. Catalan MJ, Honda M, Weeks RA, Cohen LG, Hallett M, The functional neuroanatomy of simple and complex sequential finger movements: a PET study. Brain, 1980; 121: 253-264.

15. Cavanna A, Trimble M. The precuneus: a review of its functional anatomy and behavioural correlates. Brain 2006, 129; (Pt 3): 564–83.

16. Çermika TF, Tunab H, Kayaa M, Tunab F, Gültekina A, Necmi Yiğitbaşıa O, Alavic A. Assessment of regional blood flow in cerebral motor and sensory areas in patients with spinal cord injury. Brain Research. 2006; 1109:54-59.

17. Christopoulos GI; Tobler PN; Bossaerts P; Dolan RJ; Schultz W.Neural Correlates of Value, Risk, and Risk Aversion Contributing to Decision Making under Risk. J Neurosci, 2009; 26 (24): 6469-6472.

18. Cramer SC, Lastra L, Lacourse MG, Cohen MJ. Brain motor system function after chronic, complete spinal cord injury. Brain. 2005;128:2941-2950.

19. Curt A, Bruehlmeier M, Leenders KL, Roelcke U, Dietz V. Differential effect of spinal cord injury and functional impairment on human brain activation. J Neurotrauma. 2002b;19:43-51.

20. Damasio AR. Descartes' error: emotion, reason and the human brain. 1994. New York: Grosset/Putnam.

21. Damoiseaux, J.S., Rombouts, S.A., Barkhof, F., Scheltens, P., Stam, C.J., Smith, S.M., Beckmann, C.F., 2006. Consistent resting-state networks across healthy subjects. Proc. Natl. Acad. Sci. U. S. A 103, 13848-13853.

22. De Luca, M., Smith, S., De Stefano, N., Federico, A., Matthews, P.M., 2005. Blood oxygenation level dependent contrast resting state networks are relevant to functional activity in the neocortical sensorimotor system. Exp. Brain Res. 167, 587-594.

23. Fecteau S, Pascual-Leone A, Zald DH, Liguori P, Théoret H, Boggio PS, Fregni F (2007). Activation of prefrontal cortex by transcranial direct current stimulation reduces appetite for risk during ambiguous decision making. J Neurosci 27 (23): 6212-6218.

24. Fields, Douglas. White Matter. Scientific American, 2008; 298 (3): 54-61.

25. Filippini N, McIntosh BJ, Hough MG, Goodwin GM, Frisoni GB, et al. Distinct patterns of brain activity in young carriers of the APOE-ε4 allele. Proc Natl Acad Sci USA. 2009; 106:7209-7214.

26. Fox MD, Snyder AZ, Vincent JL, Corbetta M, Van Essen DC, Raichle ME. The human brain is intrinsically organized into dynamic, anticorrelated functional networks. Proc Natl Acad Sci USA 2005; 102:9673-9678.

27. Fransson P. Spontaneous low-frequency BOLD signal fluctuations: an fMRI investigation of the restingstate default mode of brain function hypothesis. Hum Brain Mapp 2005;26:15-29.

28. Freund P, Schmidlin E, Wannier T, Bloch J, Mir A, et al. Nogo-A-specific antibody treatment enhances sprouting and functional recovery after cervical lesion in adult primates. Nat Med. 2006; 12:790-792.

29. Freund, P, Weiskopf, N, Ward, N, Hutton, C, Gall, A, Ciccarelli, O, Craggs, M, Friston, K, Thompson, A. Brain, March 2011. 134:6.

30. Frost SB, Barbay S, Friel KM, Plautz EJ, Nudo RJ. Reorganization of remote cortical regions after ischemic brain injury: a potential substrate for stroke recovery. Journal of Neurophysiology. 2003; 89(6):3205-3214.

31. Garrity A, Pearlson GD, McKiernan K, Lloyd D, Kiehl KA, Calhoun VD. Aberrant 'default mode' functional connectivity in schizophrenia. Am.J.Psychiatry. 2007; 164(3):450-457.

32. Giorgio A, Portaccio E, Stromillo ML, Marino S, Zipoli V, Battaglini M, Blandino A, Bartolozzi ML, Siracusa G, Amato MP, De Stefano N.Cortical functional reorganization and its relationship with brain structural damage in patients with benign multiple sclerosis. Multiple Sclerosis. 2010; 16:1326-34.

33. Greicius MD, Krasnow B, Reiss AL, Menon V. Functional connectivity in the resting brain: a network analysis of the default mode hypothesis. Proc Natl Acad Sci U S A 2003;100:253-258.

34. Grafton ST, Fagg AH, Arbib MA. Dorsal premotor cortex and conditional movement selection: a PET functional mapping study. J Neurophysiol, 1998; 79: 1092-1097.

35. Gulani V, Webb AG, Duncan ID, Lauterbur PC. Apparent diffusion tensor measurements in myelin deficient rat spinal cords. Magn Reson Med 2001; 45:191-195.

36. Gusitn, S, Wrigley, P, Henderson, L, Siddall, P. Brain circuitry underlying pain in response to imaged movement in Spinal Cord Injury. Pain, March 2010. 148:3.

37. Hains B. C., Black J. A., Waxman S. G. Primary cortical motor neurons undergo apoptosis after axotomizing spinal cord injury. J. Comp. Neurol. 2003; 462:328-341.

38. Hanakawa T, Honda M, Okada T, Fukuyama H, Shibasaki H. Neural correlates underlying mental calculation in abacus experts: a functional magnetic resonance imaging study. NeuroImage, 2003a; 19: 296-307.

39. Hanakawa T, Immisch I, Toma K, Dimyan MA, Van Gelderen P, Hallett M. Functional properties of brain areas associated with motor execution and imagery. J Neurophysiol, 2003b; 89: 989-1002.

40. Henderson L, Gustin S, Macey P, Wrigley P, Siddall P. Functional Reorganization of the Brain in Humans Following Spinal Cord Injury: Evidence for Underlying Changes in Cortical Anatomy. The Journal of Neuroscience. February 2011. 31:7.

41. Ivanenko YP, Poppele RE, Lacquaniti F. Distributed neural networks for controlling human locomotion: lessons from normal and SCI subjects. Brain Res Bull. 2009; 15;78(1):13-21.

42. Jeannerod M, Michel F, Prablanc C. The control of hand movements in a case of hemianaesthesia following a parietal lesion. Brain. 1984;107:899-920.

43. Jones E.G. Cortical and subcortical contributions to activity-dependent plasticity in primate somatosensory cortex. Annu. Rev. Neurosci. 2000;23:1-37.

44. Jonides J, Smith EE, Koeppe RA, Awh E, Minoshima S, Mintun MA. Spatial working memory in humans as revealed by PET. Nature, 1993; 363: 623-625.

45. Kawashima R, Roland PE, O'Sullivan BT. Functional anatomy of reaching and visuomotor learning: a positron emission tomography study. Cereb Cortex, 1995; **5** (2): 111–22

46. Kim KH, Choe SB, Haig AJ, Martin BJ. Adaptation of torso movement strategies in persons with spinal cord injury or low back pain. Spine (Phila Pa 1976), 2010; 1;35(19):1753-9.

47. Knoch D, Gianotti LR, Pascual-Leone A, Treyer V, Regard M, Hohmann M, Brugger P (2006). Disruption of right prefrontal cortex by low-frequency repetitive transcranial magnetic stimulation induces risk-taking behavior. J Neurosci 26 (24): 6469-6472.

48. Kokotilo KJ, Eng JJ, Curt A. Reorganization and preservation of motor control of the brain in spinal cord injury: a systematic review. J Neurotrauma. 2009; 26:2113-26.

49. Lotze M, Laubis-Herrmann U, Topka H. Combination of TMS and fMRI reveals a specific pattern of reorganization in M1 in patients after complete spinal cord injury. Restor Neurol Neurosci. 2006;24:97-107.

50. Lu MT, Preston JB, Strick PL. Interconnections between the prefrontal cortex and the premotor areas in the frontal lobe. J Comp Neurol, 1994: 341: 375-392.

51. Luppino G, Matelli M, Camarda R, Rizzolatti G. Corticocortical connections of area F3 (SMA-proper) and area F6 (pre-SMA) in the macaque monkey. J Comp Neurol, 1993; 338: 114-140.

52. Manning L. Do some neurological conditions induce brain plasticity processes? Behav Brain Res. 2008; 1;192(1):143-8.

53. Mattia D, Cincotti F, Mattiocco M, Scivoletto G, Marciani MG, Babiloni F. Motor-related cortical dynamics to intact movements in tetraplegics as revealed by high-resolution EEG. Hum Brain Mapp. 2006;27:510-519.

54. Maynard FM, Jr, Bracken MB, Creasey G, Ditunno JF, Jr, Donovan WH, Ducker TB, Garber SL, Marino RJ, Stover SL, Tator CH, Waters RL, Wilberger JE, Young W. International Standards for Neurological and Functional Classification of Spinal Cord Injury. American Spinal Injury Association. Spinal Cord. 1997;35:266–274

55. Mellet E, Tzourio N, Crivello F, Joliot M, Denis M, Mazoyer B (1996) Functional anatomy of spatial mental imagery generated from verbal instructions. J Neurosci 16: 6504-6512.

56. Nowak DA, Glasauer S, Hermsdörfer J. Grip force efficiency in long-term deprivation of somatosensory feedback. Neuroreport. 2003;14:1803-1807.

57. Nicotra A, Critchley HD, Mathias CJ, Dolan RJ. Emotional and autonomic consequences of spinal cord injury explored using functional brain imaging. Brain. 2006,129:718-728.

58. Oshio R, Tanaka S, Sadato N, Sokabe M, Hanakawa T, Honda M. Differential effect of double-pulse TMS applied to dorsal premotor cortex and precuneus during internal operation of visuospatial information. Neuroimage, 2010: 49(1):1108-15.

59. Picard N, Strick PL. Imaging the premotor areas. Curr Opin Neurobiol, 2001:11: 663-672.

60. Raichle ME, MacLeod AM, Snyder AZ, Powers WJ, Gusnard DA, Shulman GL. A default mode of brain function. Pro Natl Acad Sci USA. 2001; 98(2):676–682.

61. Raineteau O, Schwab ME. Plasticity of motor systems after incomplete spinal cord injury. Nat Rev Neurosci. 2001;2:263-273.

62. Ramu J, Herrera J, Grill R, Bockhorst T, Narayana P. Brain Fiber Tract Plasticity in Experimental Spinal Cord Injury: Diffusion Tensor Imaging. Exp Neurol. 2008; 212(1): 100-107.

63. Reed JL, Pouget P, Qi H-X, Zhou Z, Bernard MR, Burish MJ, Haitas J, Bonds AB, Kaas JH. Widespread spatial integration in primary somatosensory cortex. Proc Natl Acad Sci USA. 2008;105: 10233-10237.

64. Rico A, Zaaraoui W, Franques J, Attarian S, Reuter F, Malikova I, Confort-Gouny S, Soulier E, Pouget J, Cozzone PJ, Pelletier J, Ranjeva JP, Audoin B. Motor cortical reorganization is present after a single attack of multiple sclerosis devoid of cortico-spinal dysfunction. MAGMA.2011; 24-2:77-84.

65. Roelcke U., Curt A., Otte A., Missimer J., Maguire RP, Dietz V., Leenders KL. Influence of spinal cord injury on cerebral sensorimotor systems: a PET study. Journal of Neurology, Neurosurgery, and Psychiatry 1997; 62:61-65.

66. Roland PE, Skinhoj E, Lassen NA, Larsen B. Different cortical areas in man in organization of voluntary movements in extrapersonal space. J Neurophysiol, 1980; 43: 137-150.

67. Sanes JN, Suner S, Lando JF, Donoghue JP. Rapid reorganization of adult rat motor cortex somatic representation patterns after motor nerve injury. Proc Natl Acad Sci U S A. 1988; 85:2003-2007.

68. Schwab M. Repairing the injured spinal cord. Science. 2002; 295:1029–1031.

69. Schubotz RI, von Cramon DY. Functional-anatomical concepts of human premotor cortex: evidence from fMRI and PET studies. NeuroImage, 2003: 20[Suppl 1]: S120-131.

70. Scivoletto G, Ivanenko Y, Morganti B, Grasso R, Zago M, Lacquaniti F, Ditunno J, Molinari M. Plasticity of spinal centers in spinal cord injury patients: new concepts for gait evaluation and training. Neurorehabil Neural Repair. 2007; 21(4):358-65.

71. Simon SR, Meunier M, Piettre L, Berardi AM, Segebarth CM, Boussaoud D. Spatial attention and memory versus motor preparation: premotor cortex involvement as revealed by fMRI. J Neurophysiol, 2002; 88: 2047-2057.

72. Smith SM, Fox PT, Miller KL, Glahn DC, Fox PM, et al. Correspondence of the brain's functional architecture during activation and rest. Proc Natl Acad Sci U S A. 2009; 106:13040-13045.

73. Sowell ER, Peterson BS, Thompson PM, Welcome SE, Henkenius AL, et al. Mapping cortical change across the human life span. Nat Neurosci. 2003; 6:309-315.

74. Tseng GF, Prince DA. Structural and functional alterations in rat corticospinal neurons after axotomy. J Neurophysiol. 1996; 75:248-267.

75. Van den Heuvel, M., Mandl, R., Hulshoff, P.H., 2008. Normalized cut group clustering of resting-state FMRI data. PLoS. ONE. 3, e2001.

76. Wenderoth N, Debaere F, Sunaert S, Swinnen SP. The role of anterior cingulate cortex and precuneus in the coordination of motor behaviour. Eur J Neurosci, 2005; 22 (1): 235–46.

77. Wu CW, Kaas JH. Reorganization in primary motor cortex of primates with long-standing therapeutic amputations. J Neurosci. 1999; 19(17):7679-697.

78. Wyndaele M, Wyndaele JJ. Incidence, prevalence and epidemiology of spinal cord injury: what learns a worldwide literature survey? Spinal Cord. 2006; 44(9):523-529.

79. Wrigley P.J., Gustin S.M., Macey P.M., Nash P.G., Gandevia S.C., Macefield V.G., Siddall P.J., Henderson L.A. Anatomical Changes in Human Motor Cortex and Motor Pathways following Complete Thoracic Spinal Cord Injury Cerebral Cortex January 2009;19:224-232.

80. Zuo X, Kelly C, Adelstein JS, Klein DF, Castellanos FX, et al. Reliable Intrinsic Connec-tivity Networks: Test-Retest Evaluation Using ICA and Dual Regression Approach. NeuroImage. 2010;49:2163-2177.

81. http://en.wikipedia.org/wiki/File:Gray_111_-_Vertebral_column-coloured.png; Last Accessed April 24, 2012.

82. http://www.apparelyzed.com/spinalcord.html; Last Accessed April 24, 2012.

83. http://www.medwow.com/articles/wp-content/uploads/2011/05/mri_magnets.jpg ; Last Accessed April 24, 2012.